SEISMIC ANISOTROPY IN THE VAUGHAN LEWIS GLACIER JUNEAU ICEFIELD, ALASKA, 1969

Thesis for the Degree of M. S.

MICHIGAN STATE UNIVERSITY

BARRY W. PRATHER

1972

ABSTRACT

SEISMIC ANISOTROPY IN THE VAUGHAN LEWIS GLACIER, JUNEAU ICEFIELD, ALASKA, 1969

By

Barry W. Prather

Petrofabric analyses reveal that the C-axes in the hexagonal ice crystals of a glacier or ice sheet tend to align normal to the twin fabric (foliation) which is parallel to the direction of principal shear stress. From ultra-sonic experiments conducted on ice crystals under laboratory conditions, it is apparent that such preferred alignment in polycrystalline ice may facilitate a higher P-wave (compressional) velocity in directions normal to foliation.

To test the anisotropic effects in a temperate glacier with well developed flow foliation, a detailed seismic study was carried out in the summer of 1969 on the surface of the Vaughan Lewis Glacier of the Juneau Icefield. In this field experiment, a Geo-space interval timer was employed, with four three-dimensional geophones arrayed on a surface of exposed bubbly glacier ice some distance below the névé-line. The study zone was a short distance down-glacier from the last pronounced wave-bulge

(wave-ogive) below the Vaughan Lewis Icefall and presumably represented a zone of ice which had passed through a sector of intensive compressive flow and had just moved into a sector of extending flow. Also, there is an average shear stress, indicated by surface velocity measurements, that extends across the Vaughan Lewis Glacier.

Interpretation of the seismograms indicates detectable changes in seismic velocity with direction, suggesting a P-wave velocity anisotropy of 4% through a spread of 46° of measurement. A statistical Q-ellipsoid test gives a positive indication that the area measured was homogeneously anisotropic and therefore acted as a single large crystal (a theoretical inference not necessarily referring to ice per se). Examination of the P-wave data suggests that both a complex crystal orientation and layering are affecting the P-wave velocity anisotropy. The Q-ellipsoid was also used to determine that the minor axis of the velocity ellipse lies within 4° of flow foliation.

SEISMIC ANISOTROPY IN THE VAUGHAN LEWIS GLACIER JUNEAU ICEFIELD, ALASKA, 1969

By

Barry W. Prather

A THESIS

Submitted to
Michigan State University
in partial fulfillment of the requirements
for the degree of

MASTER OF SCIENCE

Department of Geology

1972

This thesis
is respectfully dedicated
to my grandparents

ALBERT A. and JESSE H. SPARKS

"Patience is a virtue,
possess it if you can.
Seldom seen in woman
and never seen in man . . ."

ACKNOWLEDGEMENTS

First and most seriously, I wish to note that the funds for this work were provided by the Committee on Research and Exploration, National Geographic Society and the Foundation for Glacier and Environmental Research. My thanks to both organizations for their support.

Secondly, and in a less serious tone, I wish to give a SINCERE THANK YOU:

To my fellow JIRPS for both patience (doing science when nearby mountains needed climbing) and carrying the necessary equipment around to do the science (high explosives were glamorous things to carry but a sledge hammer???);

To my thesis committee for a strong guiding hand in choosing the proper word at the right time (not easy when you're guiding a man whose knowledge of words is considerably less than his knowledge of anything else except women);

To Dr. Bennett for the extra trip down the Camp 18 Cleaver while the "student who was supposed to get the GT2A went off somewhere else";

To Dr. Poulter for successful instruction in the methods of dissecting high explosives with a dull knife;

To Dr. Miller for dropping his pipe into my plate of food, urging me to dump my wife into the Camp 10 water supply during a raging blizzard (a very bad mistake on my part), sending me off to Camp 8 many times in a rain or snow storm astride a vehicle that did not stand a chance of making 2 miles, let alone 20, and for what seems will be an eternal enslavement to GLACIERS;

To Mrs. Joan Miller for patience, food and cheer (she was even cheerful when a bit of poor advice from me resulted in only one broken leg for her); and

To Sharon, my wife, for the words, "Well, you had better go and get it done" and then putting up with the consequences of my going and doing.

TABLE OF CONTENTS

LIST OF TABLES

LIST OF FIGURES

Figures Page

INTRODUCTION

Glacier Geophysics Research on the Icefield

The geophysical study of glaciers has been an important part of the long-term Juneau Icefield Research Program (JIRP) since its inception in 1946 (Miller, 1952, v. section on glacier geophysics). In this regard the primary emphasis in the early years of JIRP was on the basic depth determination of key transects using seismic and gravity methods (Poulter, Allen and Miller, 1949; Miller, 1956; Thiel, La Chappelle and Behrendt, 1957; Poulter, Prather and Shaw, 1967; Prather, Schoen, Classen and Miller, 1968; and Shaw, Hinze and Asher, 1971). Since 1969, however, some selected studies have been commenced on specific aspects of the geophysical method applied to the interpretation of subsurface layering and related structures. One of these involved an electrical resistivity study of layering in the Lemon and Taku Glacier firn-pack, conducted by Heinz Miller (1972) in the summer of 1970. Another JIRP study in 1970 and 1971 employed the resistivity method for delineation of sub-surface ice bodies in frost-mounds of the Atlin area (Tallman, 1972). The third specific investigation used seismic methods to

investigate the characteristics of sub-surface structures in the Vaughan Lewis Glacier and was carried out by the writer in cooperation with H. F. Bennett (Prather and Bennett, 1972). This latter research is the subject of the present report.

Ice Petrofabric Research Pertinent to this Study

A petrofabric analysis of samples of stressed ice from glaciers and ice sheets conducted by Rigsby reveals both a single maximum and four maxima (diamond pattern) when plotted as C-axis orientation's on the Schmidt Diagram (Rigsby, 1951, 1960). In contrast, fabric studies by Gow (1963, 1964) show two, three and four maxima depending upon the depth and area from which the analyzed samples were taken. Steinemann (1954) has shown recrystallization during deformation to occur with the basal planes of ice crystals orientated in the direction of principal shear stress applied in the laboratory. Rigsby (1960) further shows that the C-axes in hexagonal ice crystals of a glacier tend to align from random orientation to a perpendicular to the direction of shear after as little as two months of applied shear stress.

Field studies of bore-hole samples in the Taku glacier by H. Bader and G. Wasserburg on the Juneau Icefield have demonstrated that in successively deeper samples, below 140 feet, there is a progressive crowding of azimuth values of the C-axes toward a line presumably

normal to the main direction of down-glacier flow (Miller, 1963, p. 132). It has also been shown in other glaciers that such fabric or foliation, alternate with zones of bubbly and clear ice (Allen, et al., 1960; Shumski, 1964; Paterson, 1969; Rigsby, 1960) with its planar direction almost normal to the preferred C-axes orientation of temperate glacier ice. Kamb (1959, 1961) has shown that the glide direction and the direction of shear stress shall never be more than a few degrees apart. Paterson (1969) points out that the ice crystal deforms by gliding on its basal plane. Therefore if the stress is long-term and large enough to produce foliation, the alignment of C-axes in polycrystalline ice probably approaches directions normal to the foliation plane. Although no successful petrofabric measurements have been made in the study area, we cannot be certain of the C-axis orientation. However, L. R. Miller (1970) while engaged in some structural glaciology research on the Vaughan Lewis glacier has extrapolated high probability that the situation in this glacier approximates that described above.

Ultrasonic Investigations of Ice

Ultrasonic laboratory studies on individual ice crystals have shown that in uniaxial crystals there is a P-wave velocity change from C-axis to A-axis of about 4% and with a maximum difference of about 7% between the P-wave velocity parallel to the C-axis and 52^{o} from the C-axis (Bennett, 1968; Green and MacKennon, 1956). Thus,

in view of the preferred alignment discussed above, as shown by petrofabric studies, and the velocity changes known to be exhibited by individual crystals, a change in velocity in polycrystalline glacier ice should be detectable between the probable C-axis orientations and the A-axis orientations (i.e., between the apparent foliation plane direction and the direction normal to foliation planes). Theoretically, changes in velocity should also be expected because of the distinct layering represented by such foliation, described by Miller (1955) as probably secondary fracture structures or flow-induced "tectonic foliation" representing a multiple system of close-spaced shear surfaces or shear zones. Postma (1956) showed that considerable anisotropy could exist with the slower P-wave velocity normal to such layers.

In this report homogeniety will be considered a uniformity in composition and physical properties between samples taken throughout a material. The sample size has a definite bearing on the criterion for homogeniety. For example, as the sample size increases in a heterogeneous material the material may be classified as homogeneous, provided the heterogeniety is uniform over large volumes. Conversely, as the sample size decreases in a homogeneous material we may eventually get to a sample size for which there is no uniformity between samples (i.e., heterogeneous). In seismic measurements the sample size is of the order of a pulse length, or in our case, 80 meters.

In this study isotropic is defined as a material whose physical properties are directionally independent. On the other hand, anisotropy is defined as the variation in physical properties of a material with direction (Jaeger, 1956). An anisotropic material whose physical properties are identical in opposite directions from a fixed reference point is defined in this study as homogeneously anisotropic. To test the possible effects of such anisotropism in relation to the seismic velocity data obtained in the field, a detailed seismic investigation was initiated on the Vaughan Lewis Glacier in 1969.

RESEARCH SETTING AND GLACIER CONFIGURATION

After preliminary tests of the field equipment on the Taku Glacier in mid-August, field work was carried out on the north side of the Vaughan Lewis Glacier, Juneau Icefield, Alaska (Figures 1 and 2, also photos in Figures 3, 4 and 5). The research area was immediately north of Camp 19--Alice's Restaurant--(Figure 2). The study area was also immediately west and down glacier from the Vaughan Lewis Icefall (Figure 6) in a zone with a well-developed flow (tectonic) foliation visible on the surface and at some depth on the walls of crevasses (Figure 7). The foliation was found to be steeply dipping and sub-parallel to the main flow direction of the glacier.

Previous Studies on the Vaughan Lewis Glacier

The desire to explain the wave bulges or wave ogives formed at the base of the Vaughan Lewis Icefall has prompted considerable study of this area which includes the M.S. theses of Freers (1966), Havas (1965), Kittredge (1967), and L. R. Miller (1970), and papers by M. M. Miller (1968), M. M. Miller, Freers, et al. (1968), M. M. Miller, Pinchak, et al. (1968), Chrzanowski (1968), Dittrich (1972)

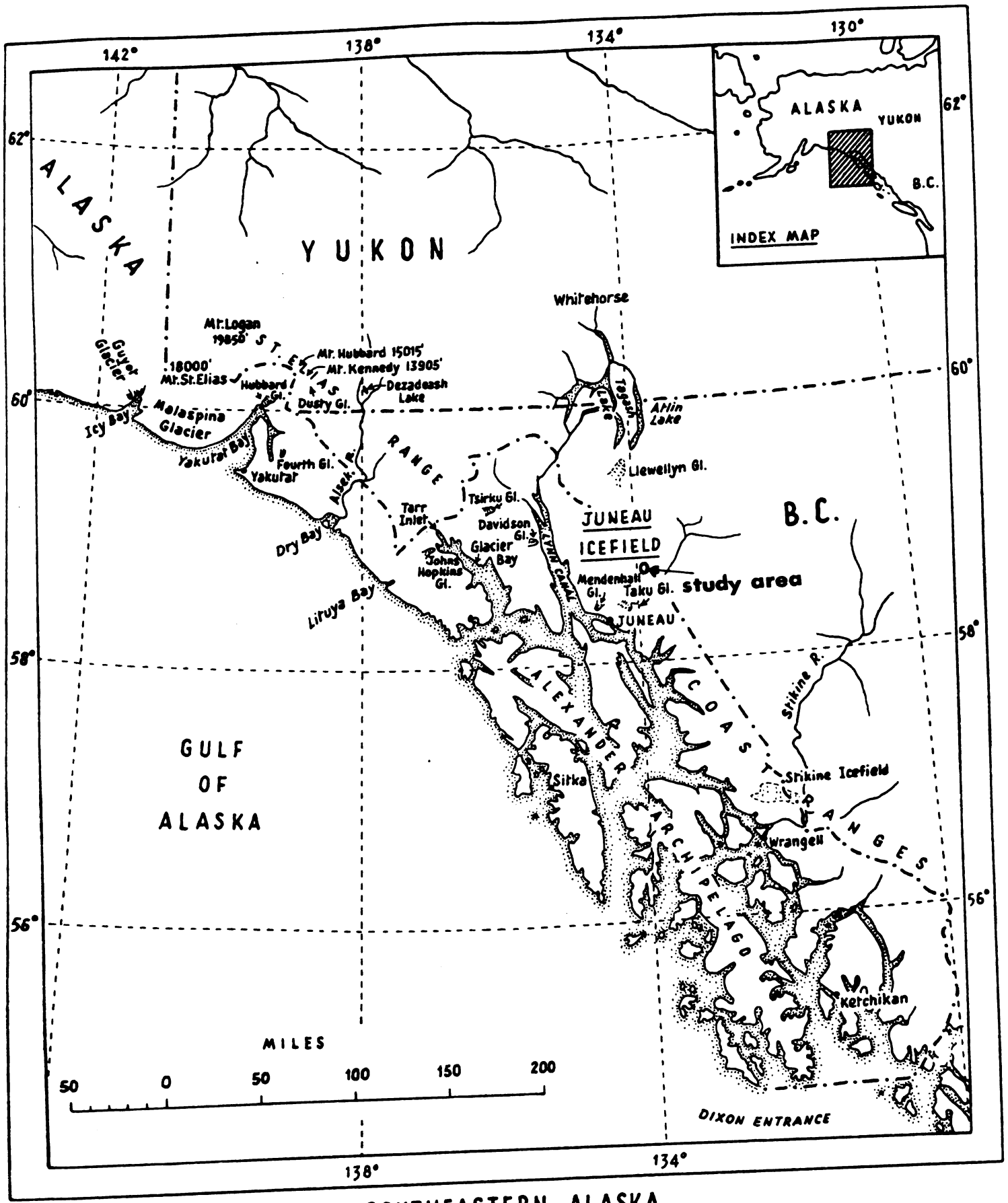

Fig. 1 SOUTHEASTERN ALASKA

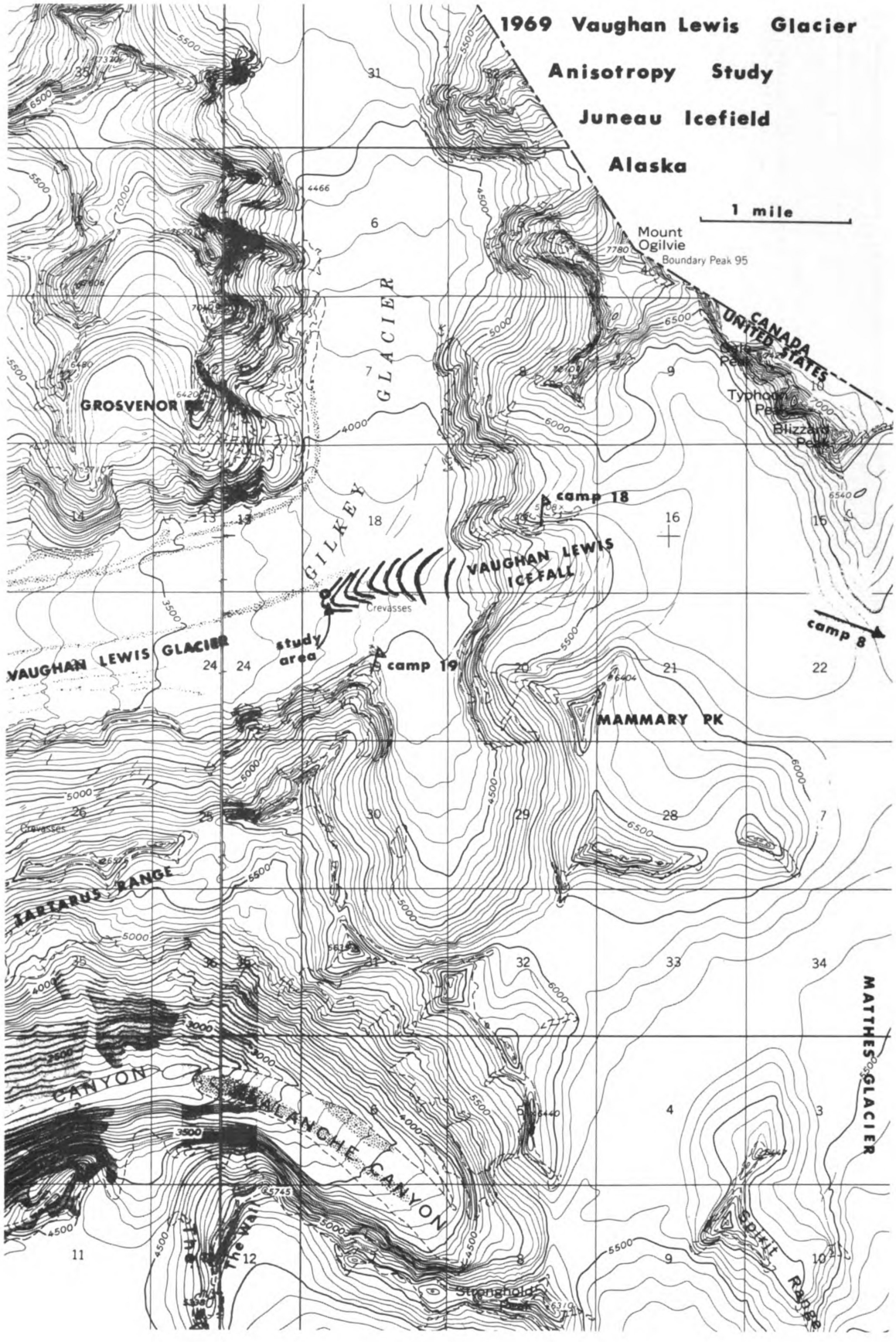
1969 Vaughan Lewis Glacier
Anisotropy Study
Juneau Icefield
Alaska
1 mile
Mount Ogilvie
Boundary Peak 95
CANADA
UNITED STATES
GROSVENOR PK
GILKEY GLACIER
camp 18
VAUGHAN LEWIS ICE FALL
Crevasses
camp 8
VAUGHAN LEWIS GLACIER
study area
camp 19
MAMMARY PK
LAZARUS RANGE
CANYON
AVALANCHE CANYON
MATTHES GLACIER
Stronghold
Spirit Range

Fig. 2

Fig. 3. Vertical air photo of the Vaughan Lewis Glacier showing wave-ogive positions in 1948 and permanent camps in 1969. (United States Navy vertical airphoto taken July 11, 1948.)

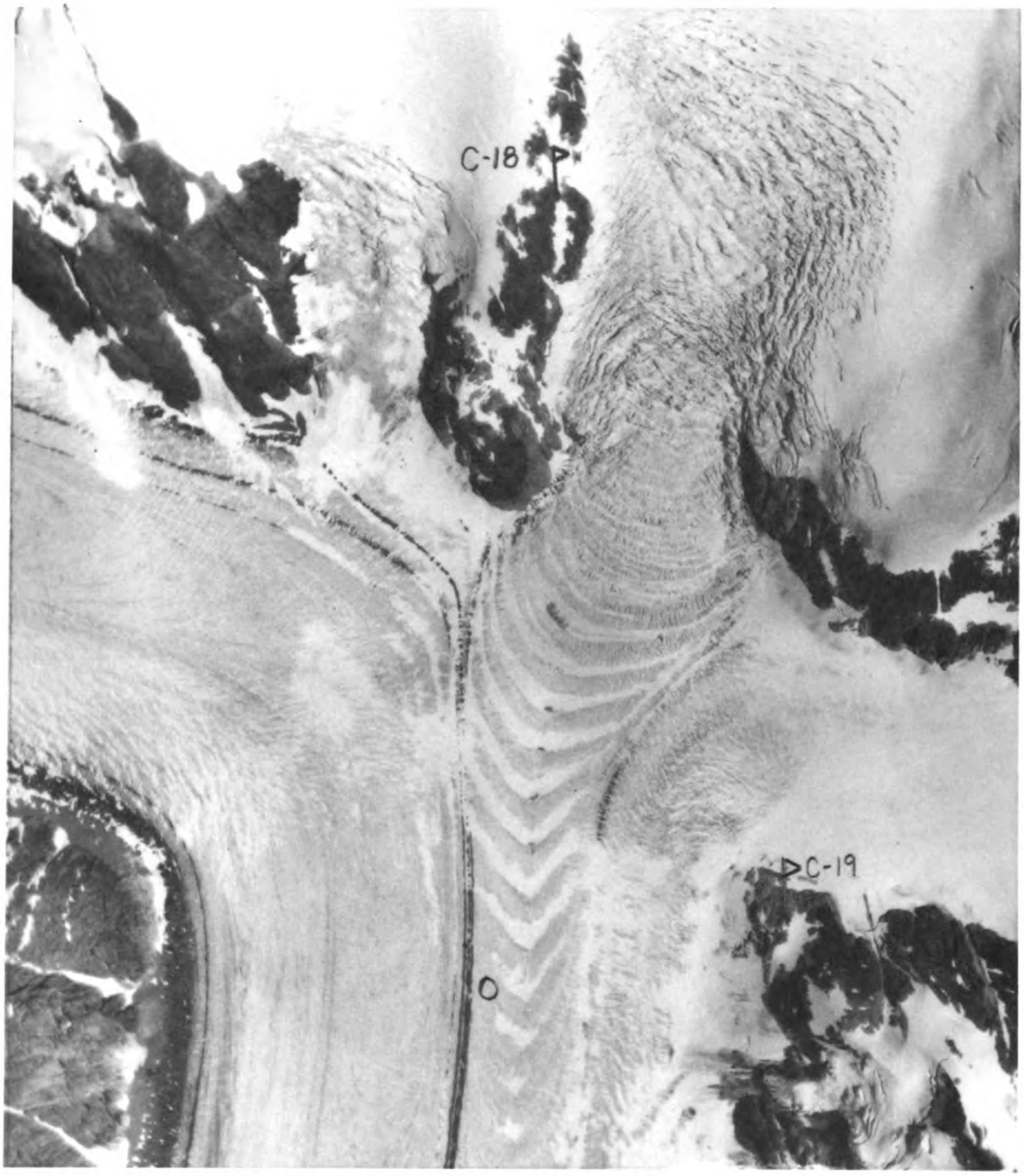
C-18
C-19
O

Fig. 4. Oblique air photo of the Vaughn Lewis Glacier, view up valley toward névé zone. (Foundation for Glacier and Environmental Research-National Geographic Society photo by M. M. Miller.)

Fig. 5. Photo view, looking east up the Vaughn Lewis Glacier toward Camp 18. Gilkey Glacier on the left, Vaughn Lewis Glacier in the center, and Unnamed Glacier on the right. (Foundation for Glacier and Environmental Research, photo by M. M. Miller.)

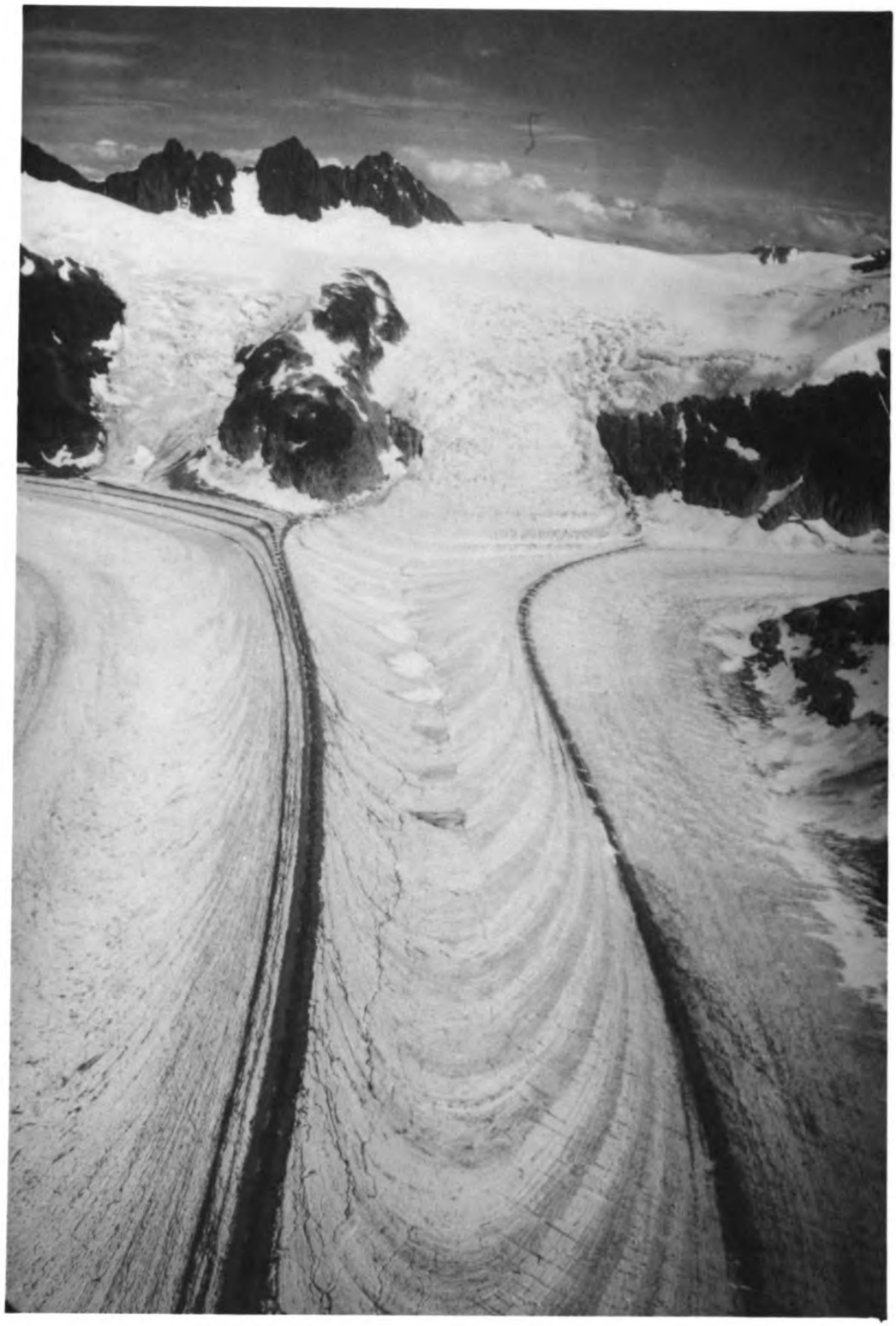

Fig. 6. Photo view looking across glacier toward Vaughn Lewis Icefall from Camp 19 showing wave-bulge zone. Unnamed Glacier in foreground. (Foundation for Glacier and Environmental Research, photo by L. R. Miller.)

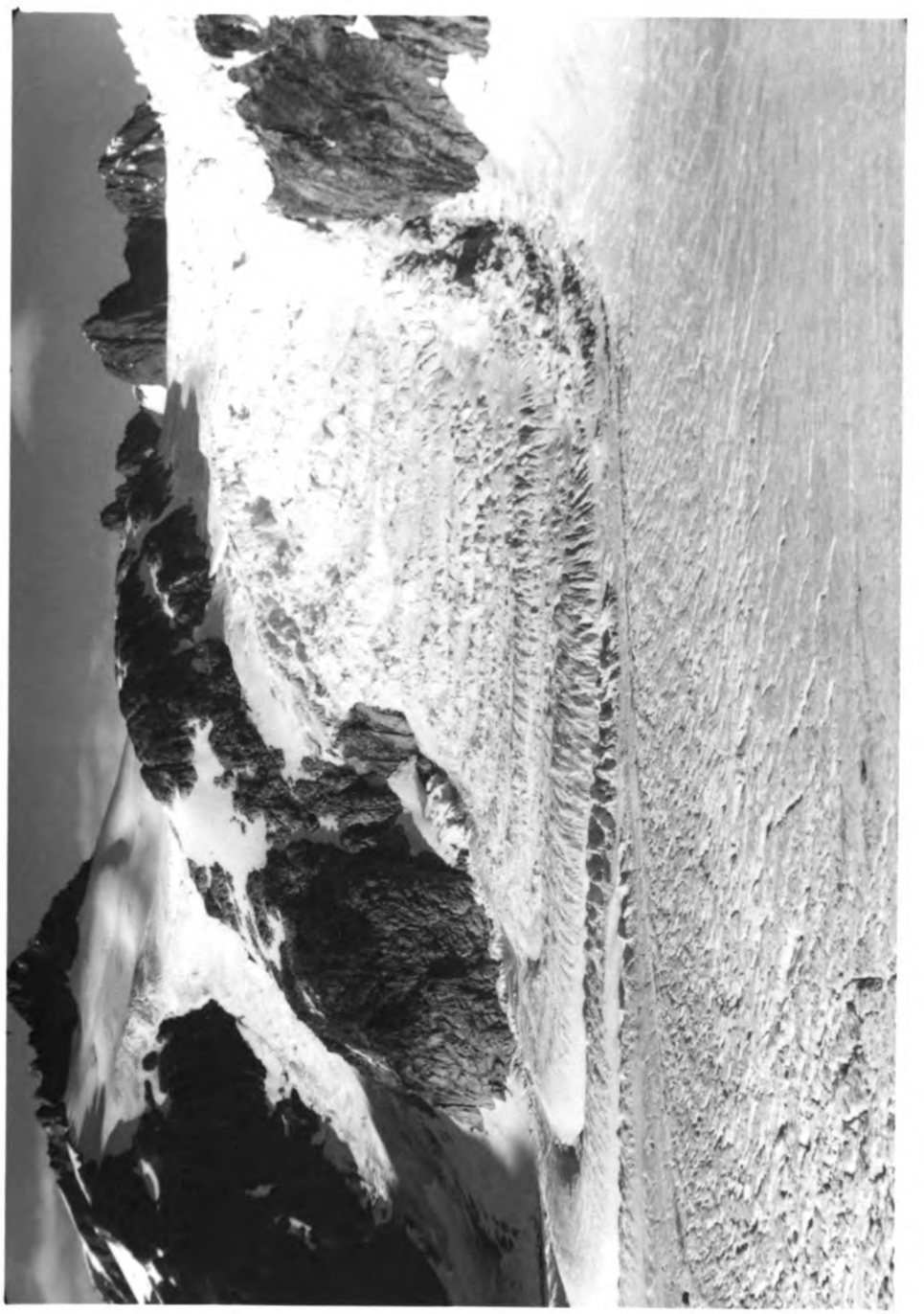

Fig. 7. Photo view of flow (tectonic) foliation in bubbly glacier ice in heavily crevassed zone outside of study area. (Foundation for Glacier and Environmental Research, photo by B. W. Prather.)

and Prather, et al. (1968). These reports address themselves to detailing the structure, movement, physical setting and theoretical causes of the ogives and wave bulges (wave-ogives). The visible macro-structures on the Vaughan Lewis Glacier with which this current investigation is concerned are well documented by Freers (1965, 1966), Kittredge (1967) and L. R. Miller (1970).

Because the wave bulges would complicate the geometry to be considered in these velocity measurements, the present study was carried out in the area immediately below the point of the last wave showing observable surface amplitude. Presumably, the compressive flow evident below the Vaughan Lewis Icefall has changed to extending flow at this point (Havas, 1965). As discussed by L. R. Miller (1968) it is predictable that beneath the steeply descending icefall, a zone of highly sheared flow folia developes close to the glacier bed. This material is subsequently folded by the extending flow and upwarped by compressional flow at the base of the icefall. In turn this is exposed, by ablation, as a series of steeply dipping shear folia. Farther down glacier additional shearing may be imposed because the Gilkey Glacier interacts with the Vaughan Lewis Glacier. In fact Dittrich (1972) has shown an approximately 3:2:1 down valley velocity differential between the Gilkey, Vaughan Lewis and Unamed Glaciers respectively. The Unamed Glacier is adjacent to the southeast of Camp 19 (Figure 2). This

means the surface of the Gilkey Glacier is moving down valley faster than, and the surface of the Unamed Glacier slower than, the Vaughan Lewis Glacier surface velocity. This interaction will produce an additional pronounced shear across the Vaughan Lewis Glacier which can result in accentuation of the tectonic foliation and crystal orientation. The magnitude of this supplemental shear across glacier is unknown because of the uncertainity of coupling between the margins of the three glaciers. Because of this and the complications introduced by the initial effects of basal shearing and subsequent deformation in a direction parallel to the main flow of the Vaughan Lewis Icefall, the stress field at the study area on the north of the Vaughan Lewis Glacier is complex and not at this time clearly understood. The foliation, however, is so well developed it is presumed to have significant effects.

To provide the simplest conditions, the study area was chosen where the foliation is sub-parallel to the remnant wave-ogive banding. This was in the approximately straight portion of the parabolic form of the remnant banding. No observed amplitude was left in the wave bands at this point and there were almost no fractures or visible inhomogenieties, such as snow, firn, or crevasses, present on the flat 3^{o} westerly dipping surface of the area measured. A very small amount of surface water was present, mostly in shallow (ten cm deep) pools and two small moulins

which were found just outside the study area. Crystals were well developed at the surface and were 0.5 to 5 cms in dimension with a predominance of smaller-sized crystals. In places they were disarticulated by ablation. As this was an ablation surface on a temperate glacier these crystal sizes are presumed to have extended well below the surface. Here, too, the foliation was pronounced so that the angles of shot lines with respect to the foliation were easily measured with a Brunton Compass for reference to the shot patterns.

Geophysical Array and Shot Directions

Three shot lines were laid out from phone number one with a 30^{o} angle between them. Distances between the ends of these three lines were measured and these distances in turn were trisected and marked, to give seven measured points from which angles and distances could be calculated (Figure 8 and Figure 9). All measurements were made to the nearest one tenth of a meter by steel tape, amounting to 0.066% accuracy of measurement. As we were only interested in relative velocities and the distances were all the same order of magnitude, no temperature correction was introduced for contraction of tape.

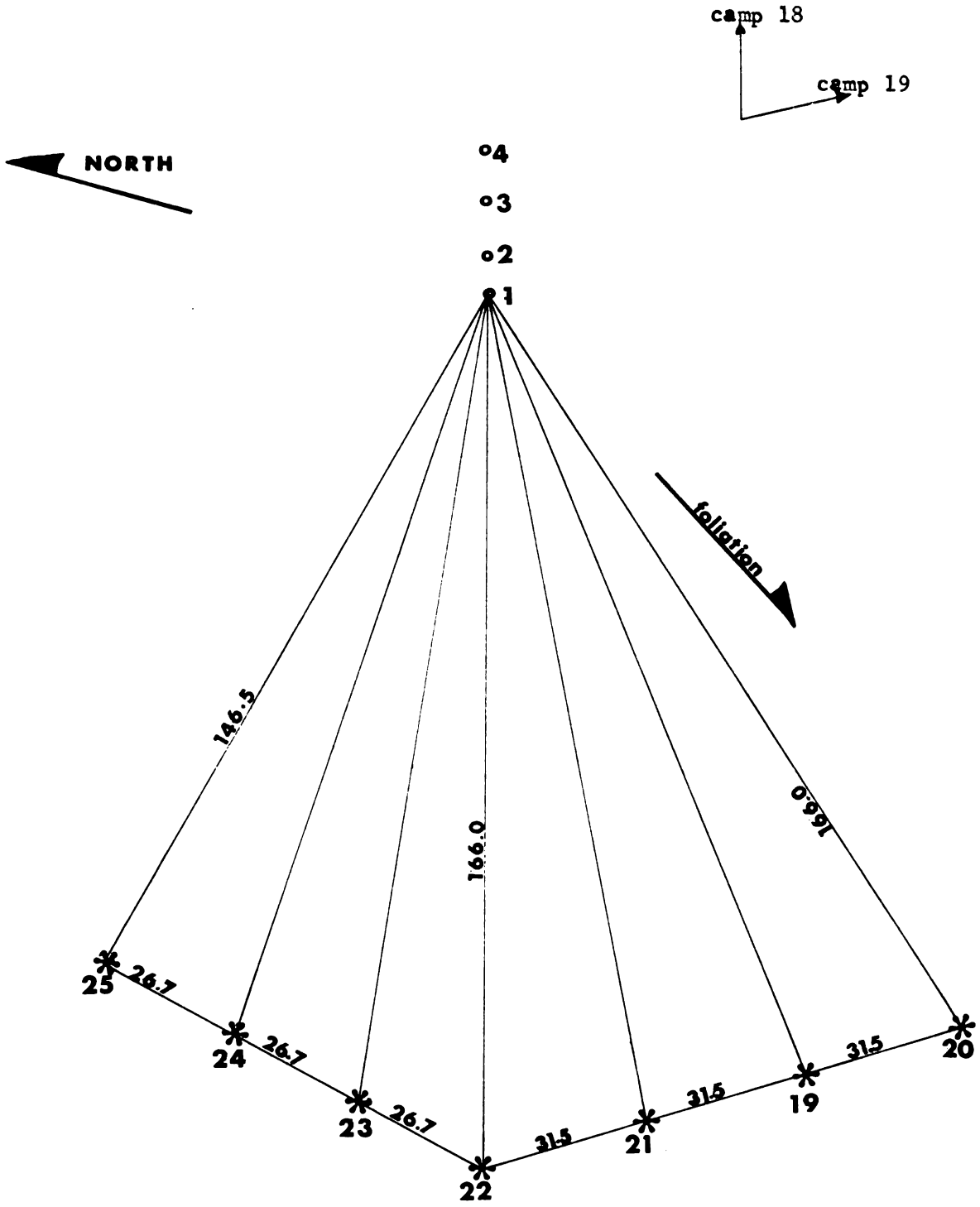

Fig. 8
Geophone and shot-point layout for the Vaughan Lewis Glacier anisotropy study. Sides dimensioned in this drawing were measured in the field to the nearest 0.1 meter.

o is three-dimensional geophone
* is shot point

meters
0 10 20 30 40 50 60

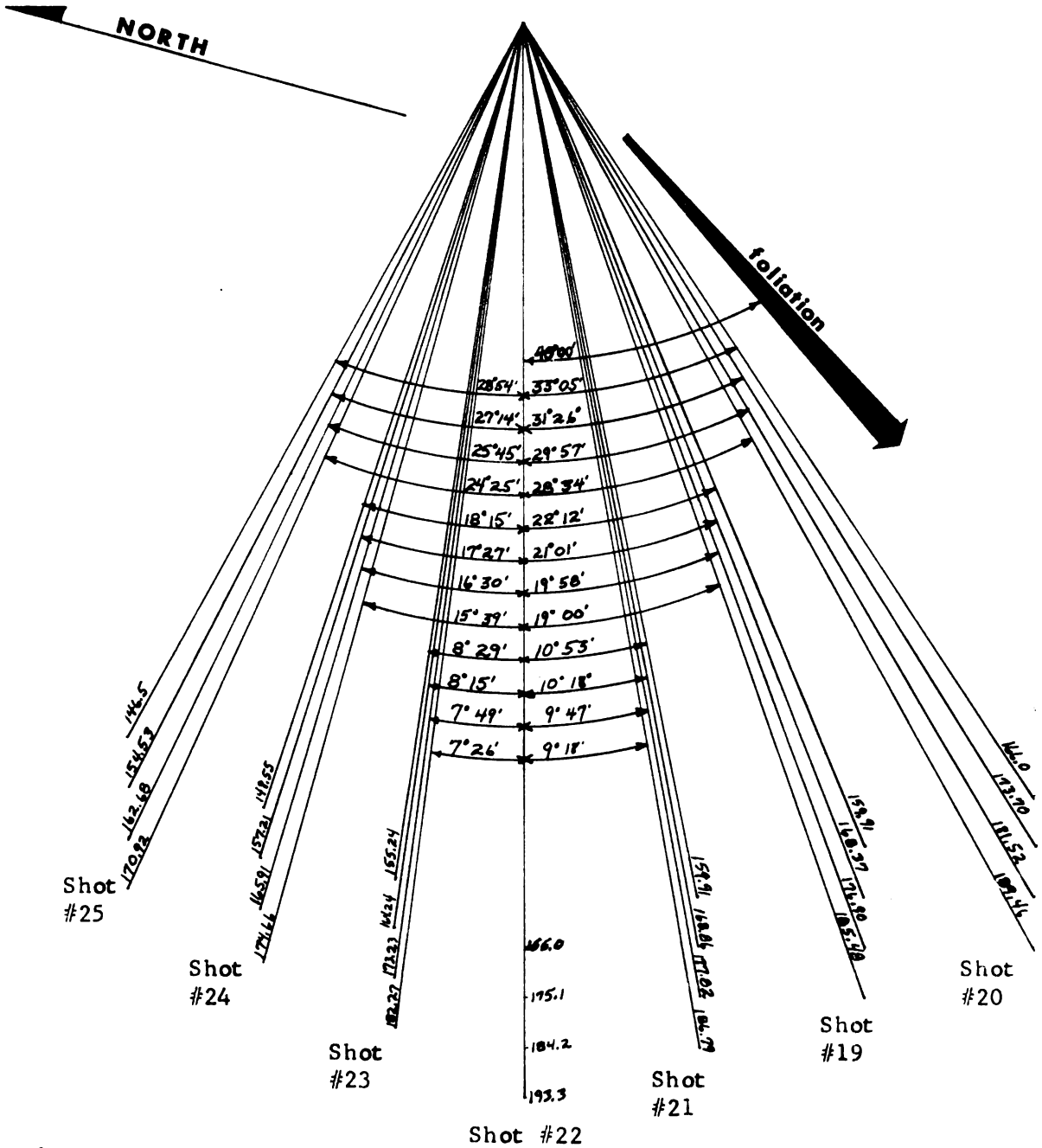

Fig. 9

Distances and relative headings from shot points to geophones for the Vaughan Lewis Glacier anisotropy study. All distances are in meters and sides labeled to 0.1 meters are measured while sides to 0.01 are calculated. Angles from shot point #22 to foliation and true north were measured with a Brunton Compass using a declination of 30 degrees E. All other angles were calculated from measured sides.

MEASUREMENT PROCEDURES IN THE FIELD

Geophones

Four three-component Geospace model 1H1 geophones were used with nearly flat response from 7 to 125 Hertz. The natural undamped frequency was 4.5 Hertz. The open circuit damping is about 25% with 510 ohm parallel resistance giving 62% damping. The X-axis of each geophone was always orientated toward the shot point. Each geophone was packed tightly with ice chips in the 7.6 cm diameter drill hole. The geophones are buried in this manner so that their tops rested several cms below the glacier surface.

Explosives

The several types of explosives used were Nitramon Primer, #8 seismic caps and 25 millisecond delay caps. A one pound charge of Nitramon Primer gave more than enough energy input to the ice for measurement, but the #8 seismic cap proved to be insufficient, so one pound charges were used throughout the study. Delay caps were also used in hopes that a pattern shot would enhance the shear wave generation, but this proved to be unsuccessful.

Shear waves, however, did appear to be enhanced by air shooting, with the charge suspended 1 to 2 meters above the surface of the ice. The delay caps also showed at least a 3 to 4 millisecond time inconsistency and so are not referenced in the records presented in this study. Shots 27 and 28 are included in Table 1, as examples of the unreliability of the 25 millisecond delay cap.

Timing and Repeatability

The interval timer used was a Geospace GT2A, slightly modified to rotate the mirror faster and give a record time of approximately 0.15 seconds. The timing lines were 10 milliseconds apart and the record time picks, by use of a magnified reticule, were estimated to 1/4 millisecond. Statistics are presented in Table 1 from several records with common shot points and geophone locations to show that the timing method is repeatable within 3/4 millisecond. Most of this error is probably in the time picking.

Record Picking

The geophones remained in the same hole throughout the period of data collection, but the X-axis was reoriented toward the shot point, with Y normal and Z vertical for each shot. All traces show a P-wave arrival, but it was weakest on the Y traces. This can be seen in the suite of records, which are arrayed by azimuth, in Figures 10 through 16.

TABLE 1.--Analysis of cap firing and time pick repeatability.

Shot vs. Shot		X Axis Trace No.	First Arrival Time Picks		m	sigma
Type #8 Seismic Cap						
13	14	1	54.0	54.0		
		2	51.0	51.0		
		3	49.0	49.5		
		4	45.5	46.0	+0.25	.3535
$\frac{13+14}{2}$	22	1	54.0	53.75		
		2	51.0	50.75		
		3	49.25	49.25		
		4	45.75	46.25	0.0	.3061
15	21	1	52.0	52.0		
		2	50.0	49.5		
		3	48.0	49.5		
		4	44.5	44.0	+0.125	.8291
16	19	1	52.0	53.0		
		2	49.5	50.5		
		3	48.0	48.0		
		4	44.0	45.0	+0.35	.866
17	18	1	54.0	53.5		
		2	51.5	51.5		
		3	49.5	49.5		
		4	46.5	46.5	-0.125	.25
$\frac{17+18}{2}$	20	1	53.75	54.25		
		2	51.5	51.0		
		3	49.5	49.25		
		4	46.5	45.5	-0.31	.625
25 Millisecond Delay Cap						
27	28	1	78.5	86.0		
		2	76.75	84.25		
		3	74.75	83.25		
		4	72.25	80.5	+7.94	7.95

where

$$m = \sum_{1}^{4} \frac{(t_2 - t_1}{4} \qquad \text{sigma} = \sum_{1}^{4} \frac{(t_2 - t_1)}{4}$$

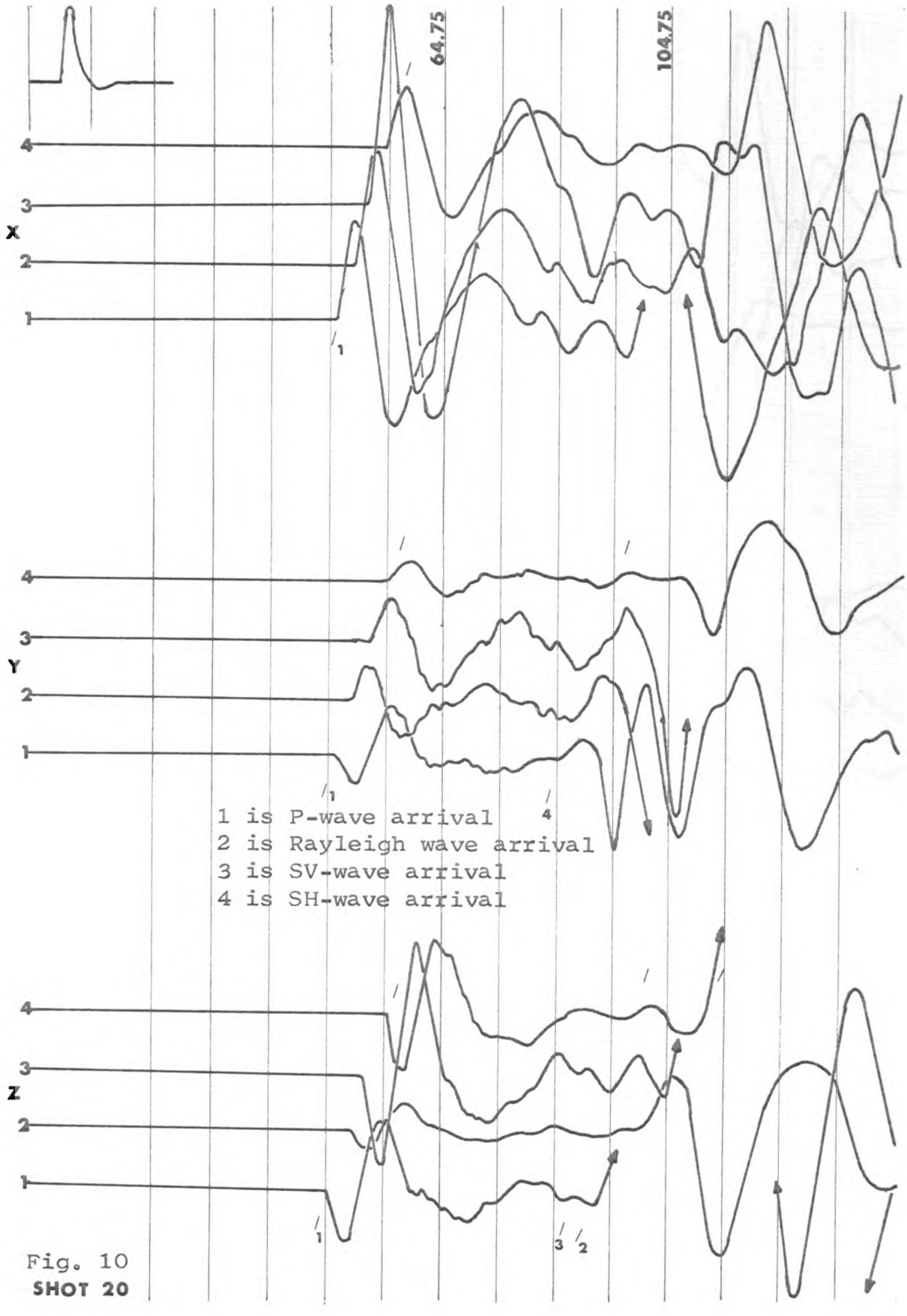

Fig. 10
SHOT 20

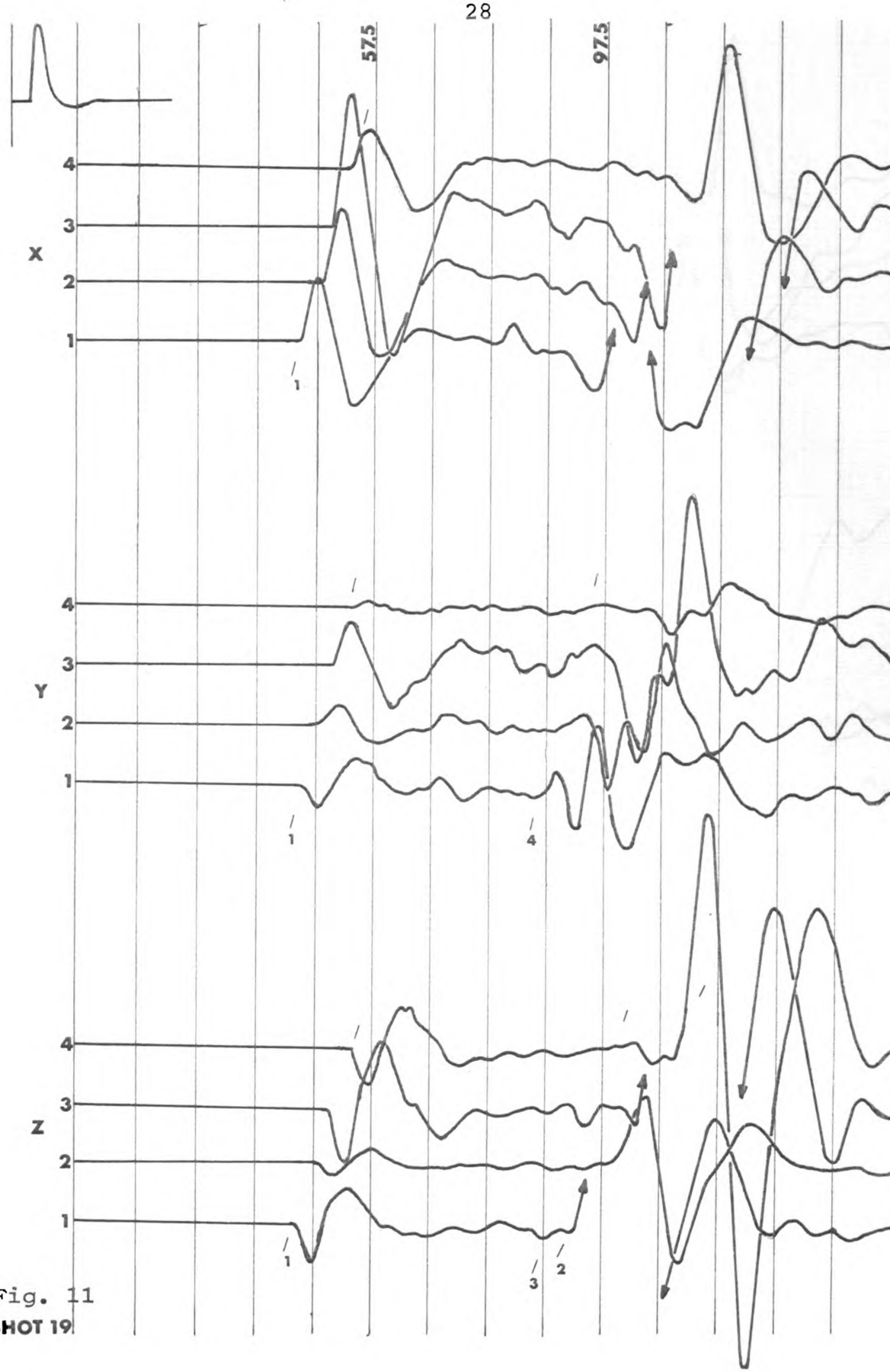

Fig. 11
SHOT 19

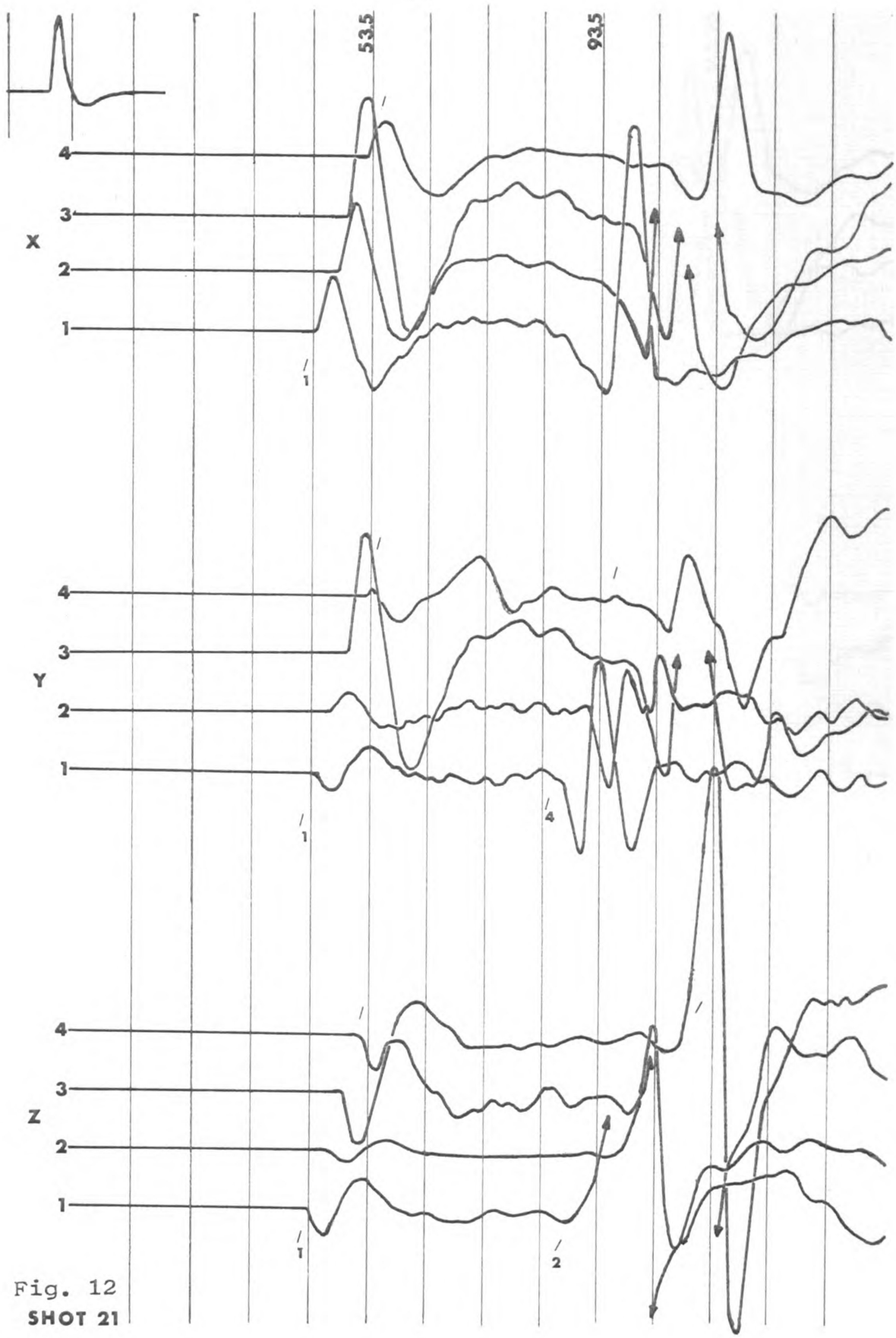

Fig. 12
SHOT 21

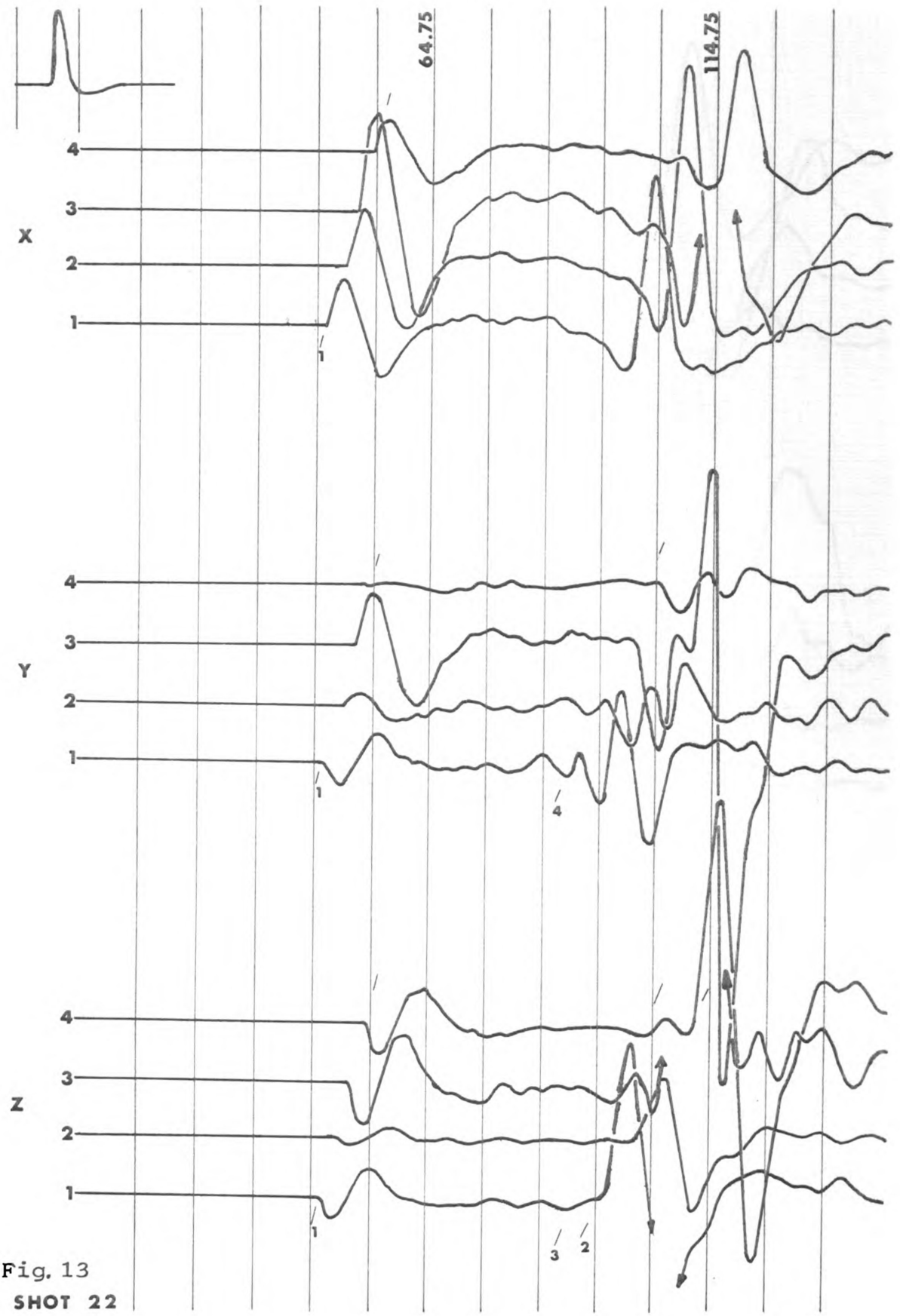

Fig. 13
SHOT 22

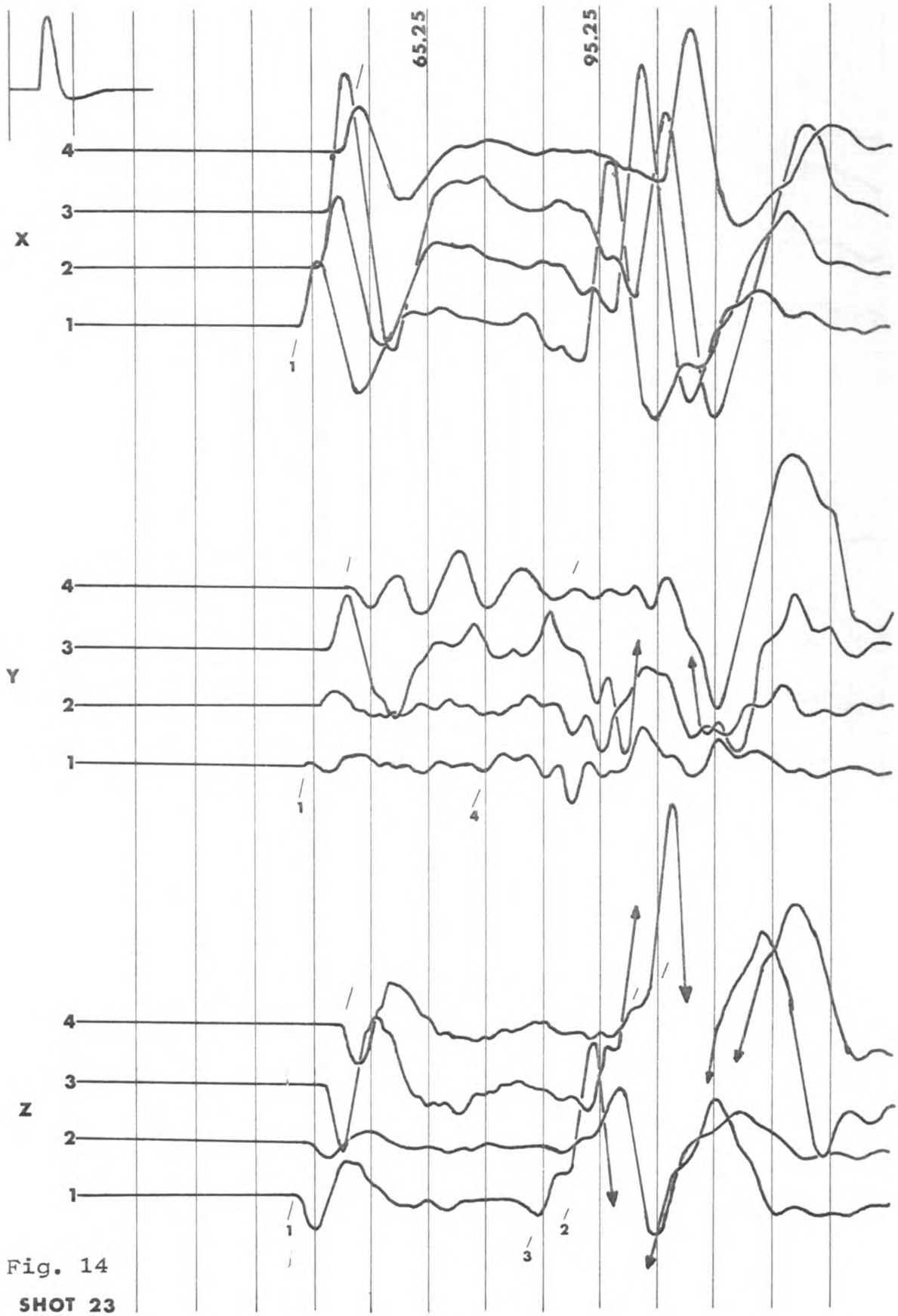

Fig. 14

SHOT 23

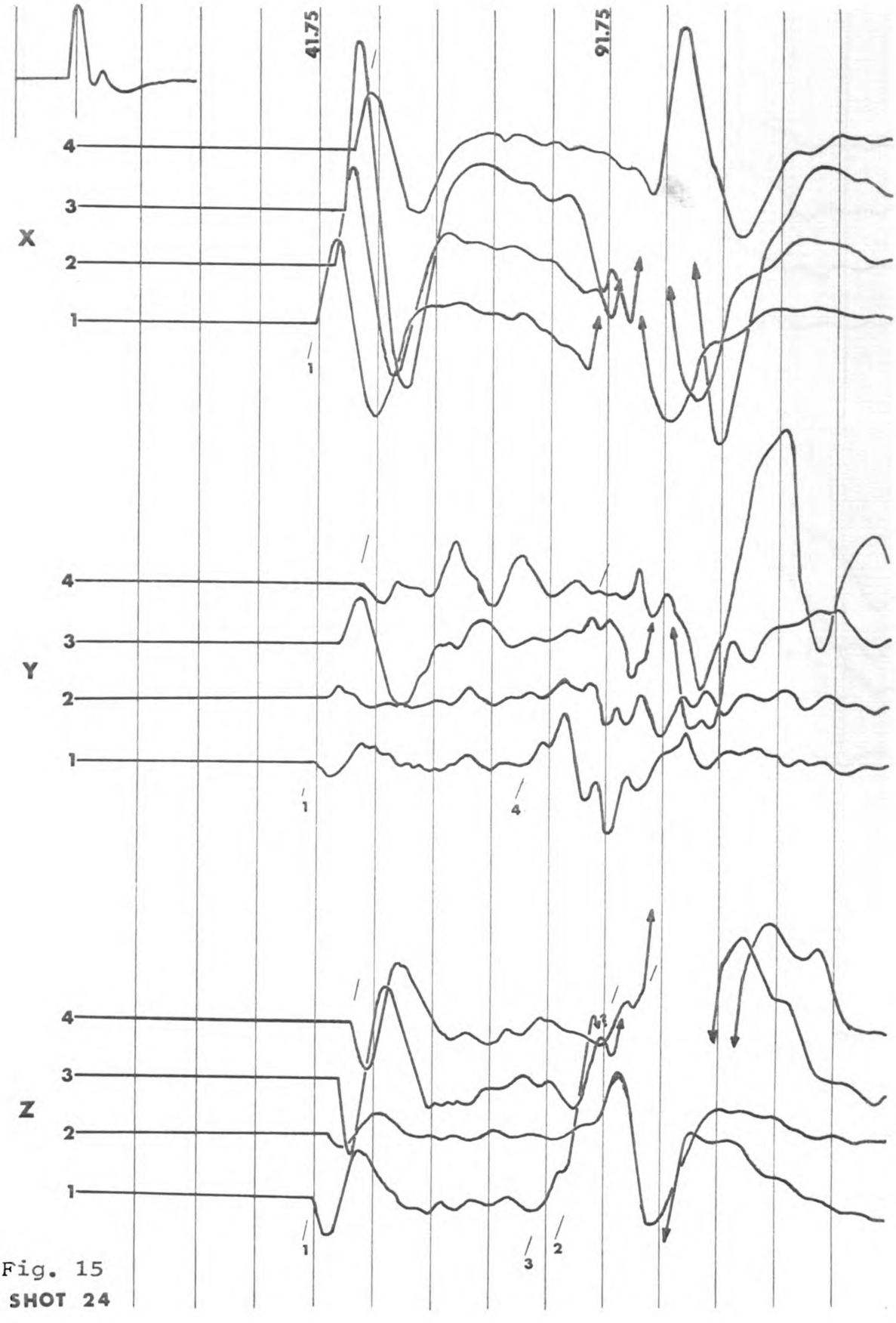

Fig. 15
SHOT 24

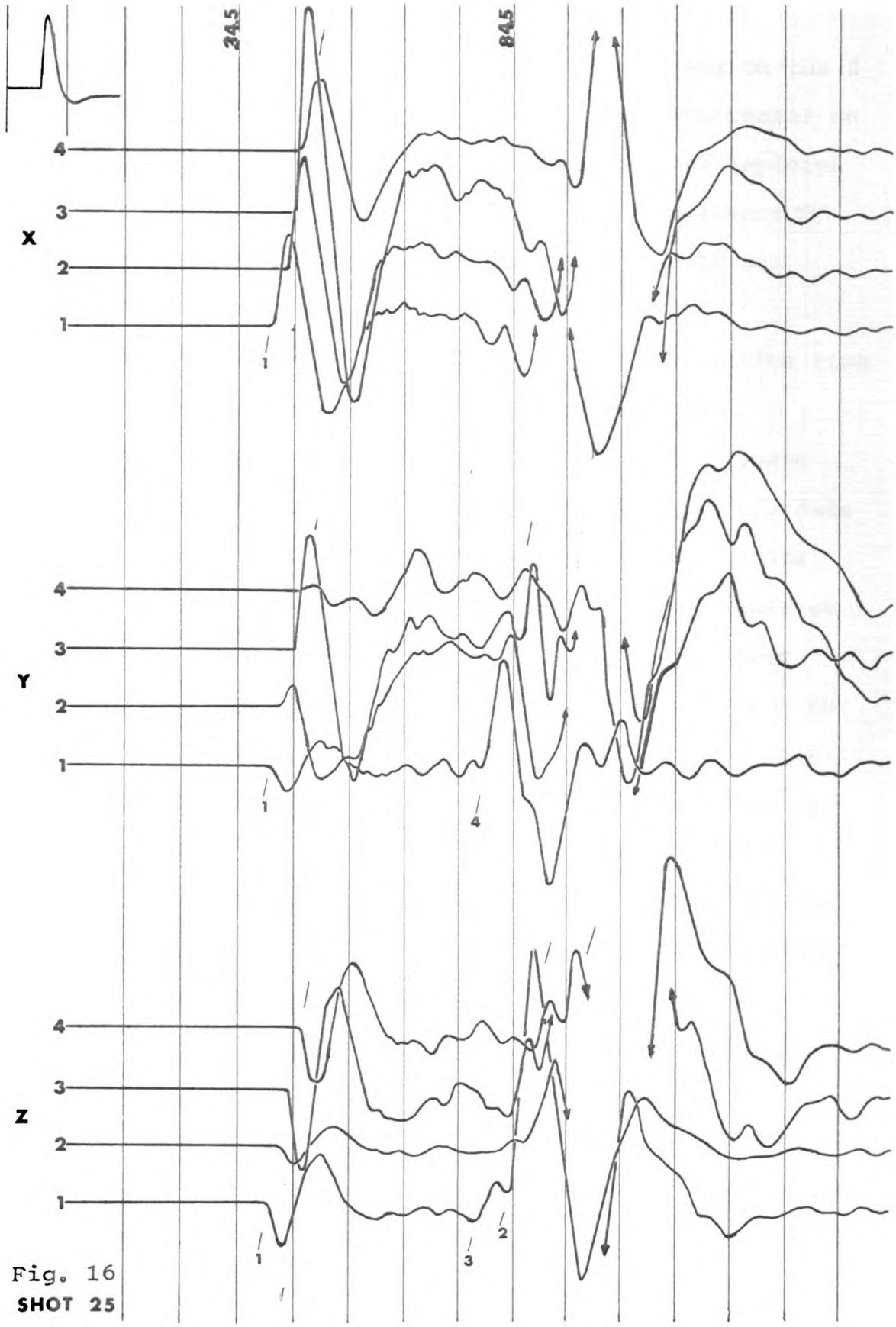

Fig. 16
SHOT 25

The Rayleigh wave arrival was very strong on the Z traces almost as strong on the X traces and much weaker on the Y trace. Some early energy, just before the Rayleigh wave, is evident on the Z traces, which may represent SV-wave arrivals. For comparison, this energy trace was picked on all but record 21.

The P-wave arrivals were easiest to pick. The time was picked at the point where each individual trace deviated from zero displacement. The individual P-wave arrivals on the X traces were used in the preliminary data reduction to find if further analysis would be of value. The Rayleigh wave arrivals were picked on the Z traces at the point the trace started to swing into its steepest slope. This point was then brought down perpendicular to a zero displacement line. All records but those at shot 21 were also picked for SV-wave arrivals on the Z traces. This energy was assumed to appear on the record just before the Rayleigh wave arrival and the points where the trace began to swing were brought to the zero displacement line on a perpendicular. By comparing the SV and Rayleigh wave arrivals on all records, except 21, a mean velocity ratio of $V_R/V_S = .9327$ was computed. This compares favorably with Knopoff (1952) for a Poissons Ratio of 0.33, the calculated value from $\overline{V}_P$, $\overline{V}_S$ in our area. This calculation for Poissons Ratio is based on the assumptions that the material is linearily elastic and isotropic. The SV-wave velocity was then computed by dividing the Rayleigh

wave velocity by .9327 for all seven records. This was done because the Rayleigh picks were more uniform and easier to pick. Although a velocity ratio of .9327 may introduce slight errors in an absolute velocity determination, the relative velocity will not be changed.

The SH-wave arrivals were the most difficult to pick. It was assumed that a Love wave arrival was observed on the Y trace immediately before the Rayleigh wave arrival and that the beginning of this wave train was the SH-wave arrival. Records 23, 24 and 25 are extremely poor for SH-wave arrivals and the picks are not obvious. On record 22 only one trace was picked for the SH-wave. Because this study required only relative wave velocities, greater care was taken to pick the same event on each record rather than make certain that the first energy of the SH wave was picked. Better shear wave generation techniques need to be developed to further refine a study of this type. The technique of horizontal hammer blows would have been tried but for the equipment limitations with respect to timing.

P, SV and SH-wave velocities were picked by making a best straight line fit to the cross spread picks. For the P-wave, trace 2 was late. This was due to poor galvonometer adjustment in the field. On Figures 10 through 16, the P-wave picks are marked with a number 1, the Rayleigh wave picks are noted as number 2, the SV-wave picks as number 3, and the SH-wave picks are marked as number 4.

PRELIMINARY MEASUREMENT AND ANALYSIS

Prior to making directional measurements for anisotropy, a detailed refraction line was recorded on the shot 22 heading (Figure 10) to establish that the ray paths in the study represented direct arrivals traveling near the ice surface. The time-distance curve (Figure 18) for this line shows a very straight line which means there is no detectable vertical velocity gradient and therefore the ray paths were indeed near the surface. From previous reflection records (Prather, et al., 1968; Kittredge, 1967), the depth of the Vaughan Lewis Glacier at the study area has been determined to be about 200 meters. Assuming an upper limit bedrock P-wave velocity of 6,000 meters per second and a P-wave velocity for ice of 3,500 meters per second, the critical distance is about 775 meters. This coupled with the refraction line data indicates that we are sampling a single layer during the anisotropy measurements over distances that are less than 200 meters.

Two cross-spread measurements, shots 31 and 32, were made using 12 vertical component phones. The time-distance curves for these two measurements are shown in

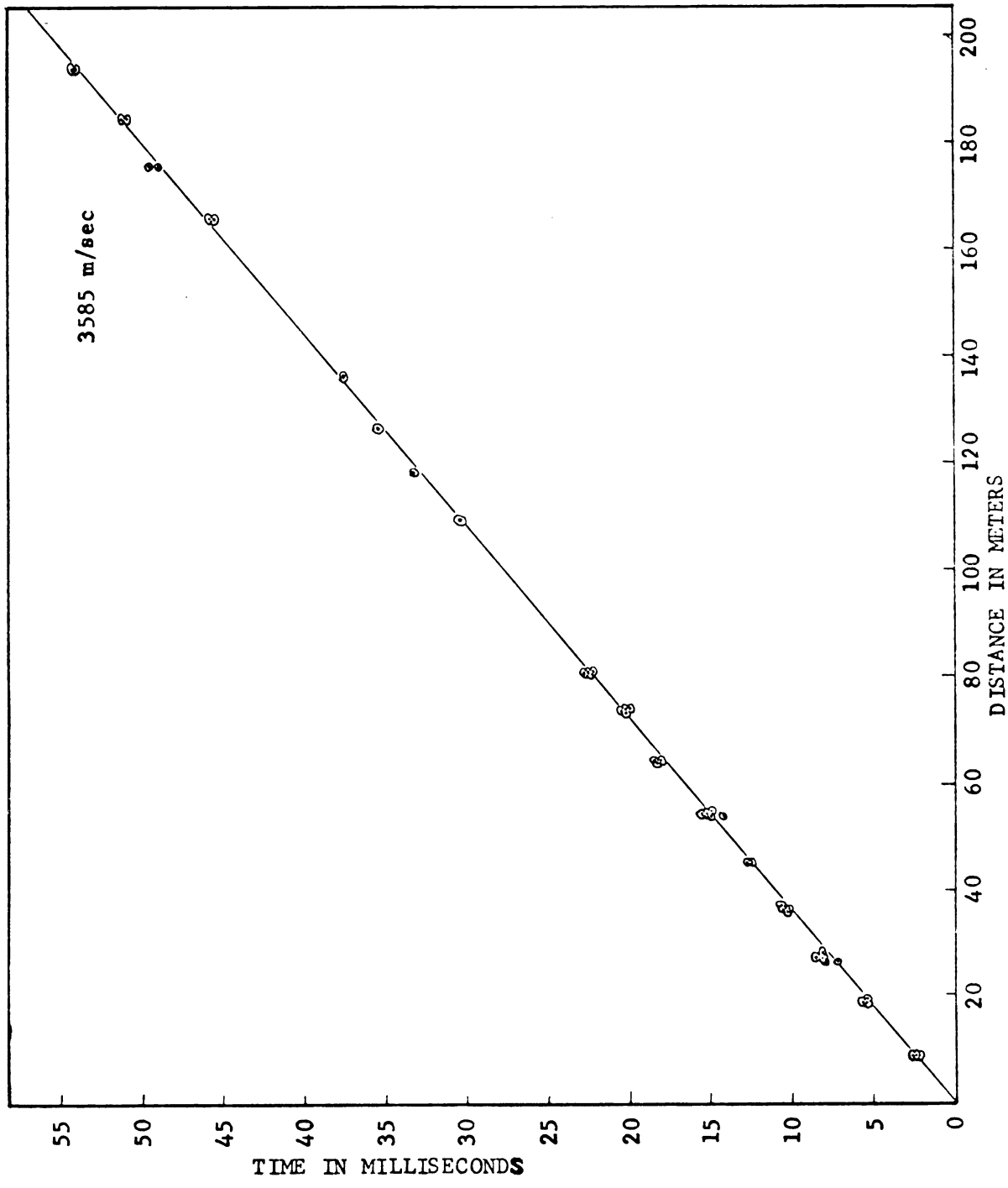

Fig. 17. Time-distance curve for first arrivals of shots one thru fourteen on the Vaughan Lewis Glacier, 1969.

Figures 19 and 20. The P-wave velocity measurements in Figure 19 compares favorably with the detailed refraction line of Figure 12, and is 6% lower than earlier vertically orientated P-wave velocity data from the Taku Glacier (Poulter, 1949). The Rayleigh wave velocity of Figure 14 shows nearly 5% difference from the data from shot number 22. The amplifier gain was turned down to a minimum value for shot number 32 and the picks could have been inaccurate enough to explain this discrepancy. Also, the record length was longer (i.e., 0.4 seconds) which reduced the accuracy of the time determination.

The P-wave velocities determined from the directional experiment, which included records 19 through 25, were plotted as a function of azimuth and are shown in Figure 21. Both individual phone and array velocities are plotted in this figure. An estimated straight-line fit to the data is included on the figure which is not a least squares or computed fit. Since the plot showed P-wave velocity anisotropy, the P, SV and SH data were then statistically fitted to a Q-ellipsoid (Bennett, 1972) following the method of Nye (1957).

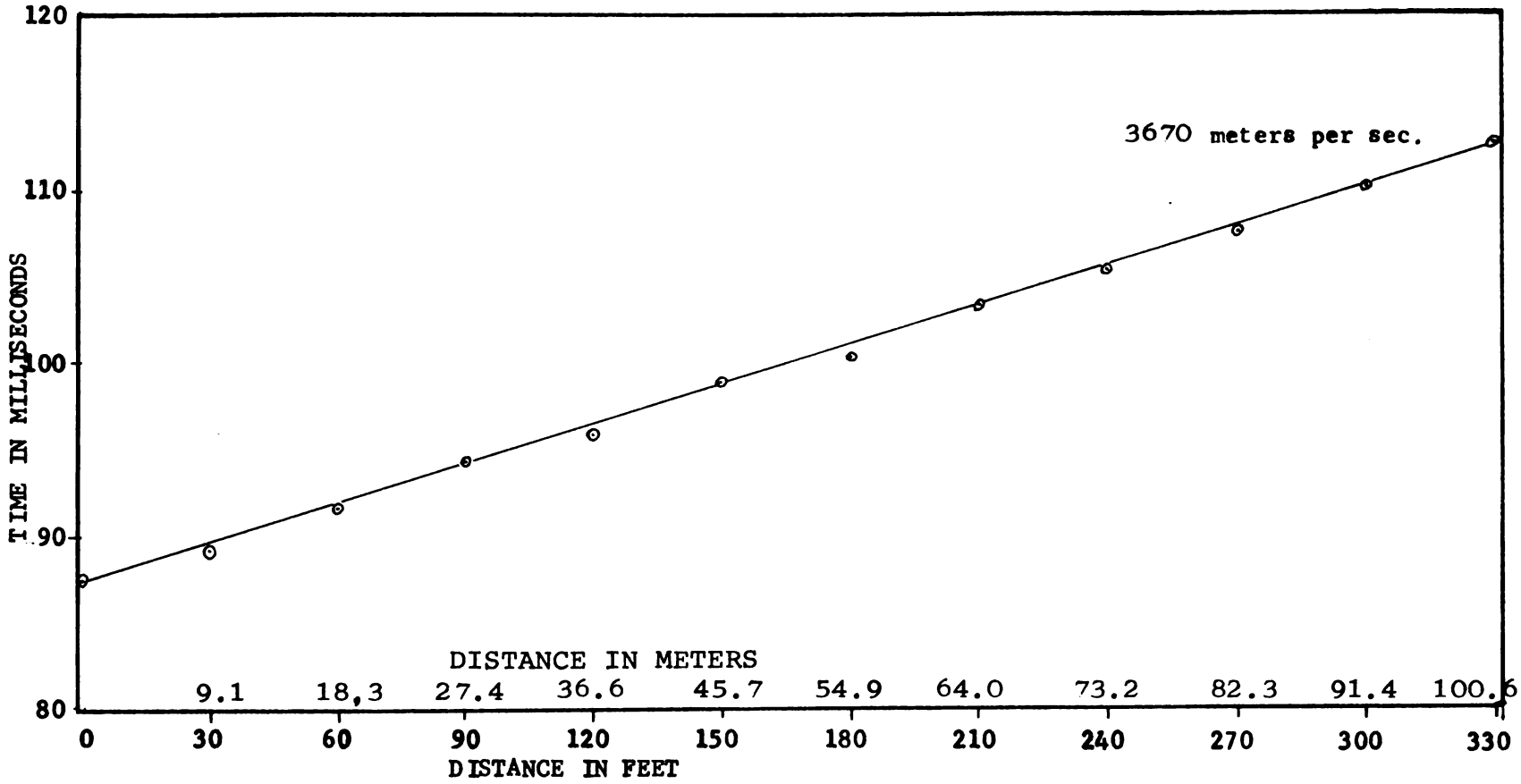

Fig. 18. P-wave time-distance curve of shot 31. Velocity in meters per second is computed from approximately 12,210 feet per second. The shot point is in a moulin about 172 meters from geophone one or zero distance. The 12 geophones used in this cross spread measurement have a vertical axis only.

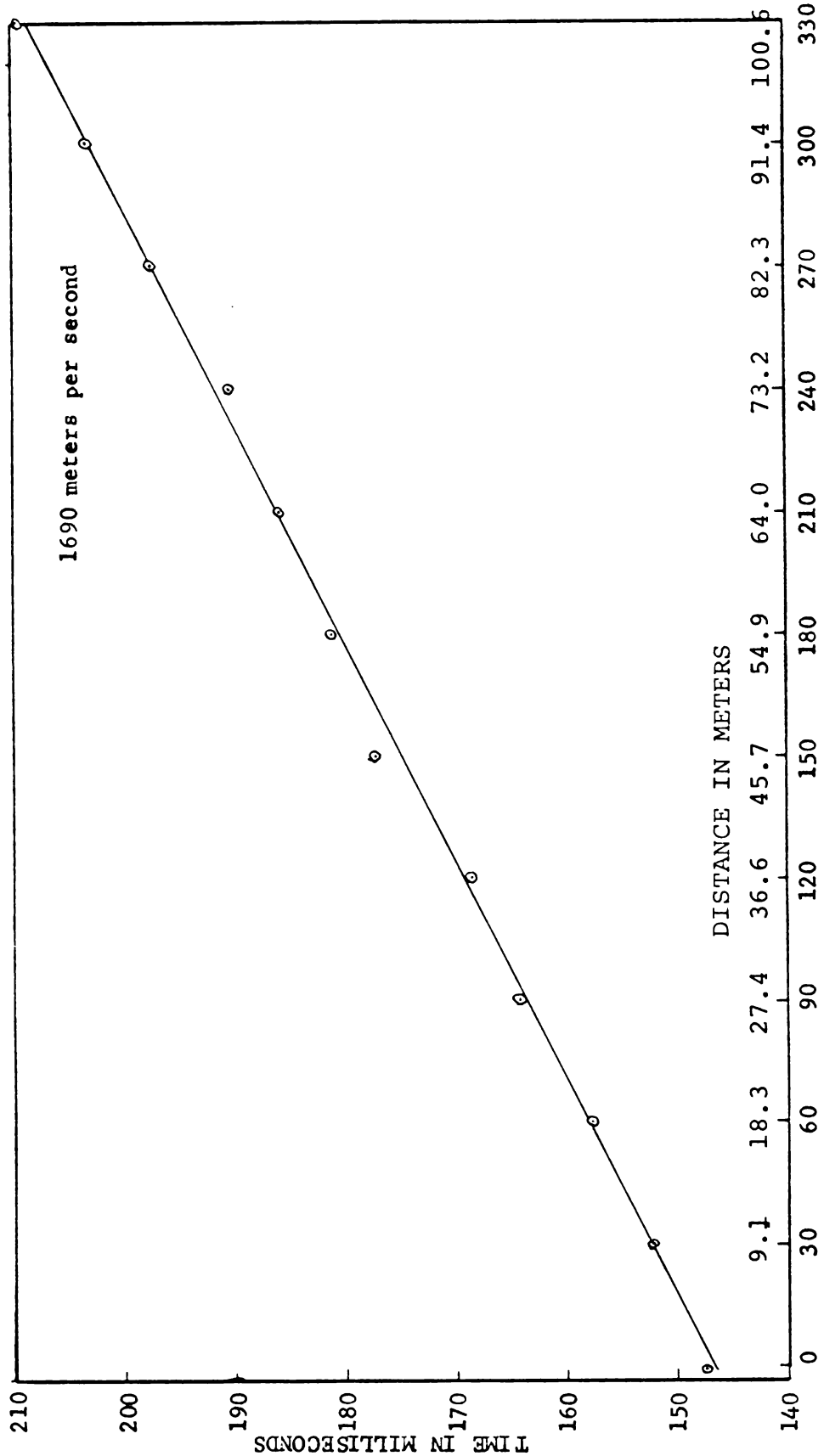

Fig. 19. Rayleigh wave cross spread time-distance curve with 12 vertical axis geophones (Shot 32). The shot point is in a moulin about 172 meters from geophone one or zero distance on this graph. Velocity in meters per second is computed from 5,540 ft./sec.

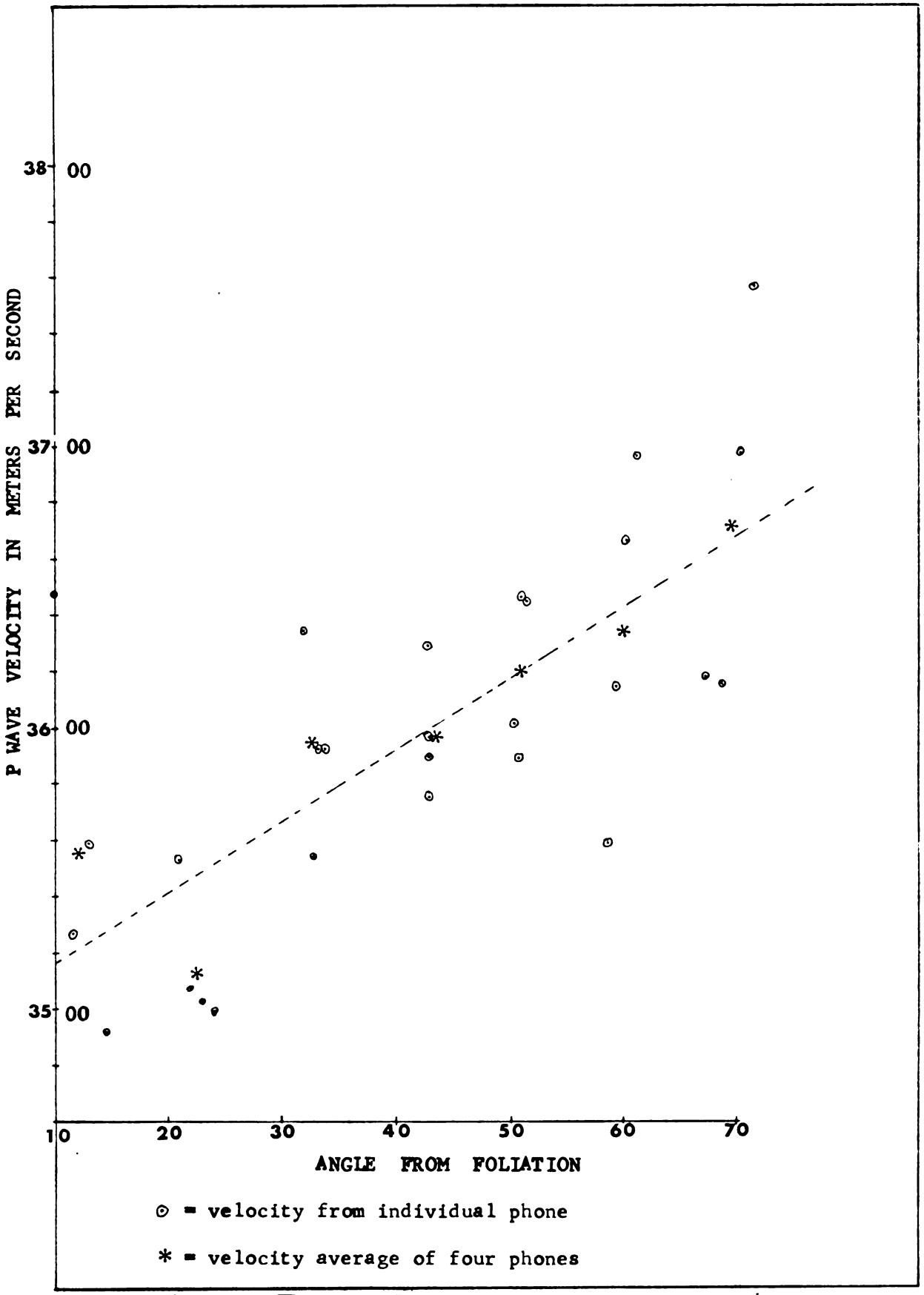

Fig. 20 Preliminary directionsl P-wave analysis.

THE Q-ELLIPSOID TEST FOR ANISOTROPY AND RELATED STATISTICS

Q-Ellipse Definitions

A Q-ellipsoid is a simple elastic stiffness figure derived by Bennett (1972) from elastic wave theory in anisotropic media and is defined as:

$$Q = \rho \ (V_1^2 + V_2^2 + V_3^2)$$

where ρ is density and V_1 is compressional or P-wave phase velocity. V_2 and V_3 are the two psuedo shear-wave phase velocities that are possible for anisotropic material. The P-wave velocity is about twice as great as either of the two shear-wave velocities and therefore constitutes about 66% of the value of Q. This is fortunate because the P-wave picks are considerably more accurate in this study. The Q-ellipsoid in this paper disregards the density term because it is a constant for all tests, so that the Q is actually Q/ρ.

The values for Q are best fit to an ellipse by the method outlined by Nye (1957). The ellipse equation is given by:

$$\frac{Q}{\rho} = (V_1^2 + V_2^2 + V_3^2) = l^2 \alpha_1 + 2lm \alpha_3 + m^2 \alpha_2$$

In matrix notation:

$$\frac{Q}{\rho} = A = \boldsymbol{\theta} \boldsymbol{\alpha}$$

where:

$$A = \frac{1}{\rho} \begin{matrix} Q_1 \\ Q_2 \\ Q_3 \\ Q_4 \\ Q_5 \\ Q_6 \\ Q_7 \end{matrix} \qquad \boldsymbol{\theta} = \begin{matrix} l_1^2 & m_1^2 & l_1 m_1 \\ l_2^2 & m_2^2 & l_2 m_2 \\ l_3^2 & m_3^2 & l_3 m_3 \\ l_4^2 & m_4^2 & l_4 m_4 \\ l_5^2 & m_5^2 & l_5 m_5 \\ l_6^2 & m_6^2 & l_6 m_6 \\ l_7^2 & m_7^2 & l_7 m_7 \end{matrix} \qquad \boldsymbol{\alpha} = \begin{matrix} \alpha_1 \\ \alpha_2 \\ \alpha_3 \end{matrix}$$

The best value of $\boldsymbol{\alpha}$ is:

$$\boldsymbol{\alpha} = (\boldsymbol{\theta}_t \boldsymbol{\theta})^{-1} \boldsymbol{\theta}_t A$$

The computer program used to accomplish the matrix calculations and the square deviations is given in appendix. The analysis was accomplished on the CDC 6500 at Michigan State University.

The alpha matrix of the computer program has three terms for the plane ellipse, α_1, α_2, and α_3. The value of e for a particular direction i is then:

$$e_i = l_i^2 \alpha_1 + l_i m_i \alpha_3 + m_i^2 \alpha_2$$

where l and n are direction cosines.

Two values, $\bar{M}$ and S, are computed for statistical use. The first is the mean of the data and the second is the average of the major and minor axes of the fitted ellipse. The mean of the data is:

$$\bar{M} = 1/n \sum_{i=1}^{n} M_i$$

where for each direction i:

$$M_i = V_1^2 + V_2^2 + V_3^2$$

and the value of S from the major and minor ellipse axes is:

$$S = \tfrac{1}{2} (\alpha_1 + \alpha_2)$$

The ratio of $\bar{M}$ to S is an indicator of the uniformity of sampling. In order to determine a more reliable Q-ellipsoid, the data should be equally distributed in azimuth. This is true if $\bar{M}$ approaches S and the ratio nears 1. If S and $\bar{M}$ differ by very much, then there is an unequal distribution of data. Ideally, the measurements should be uniformly distributed over at least 180 degrees and S will then approach $\bar{M}$. In this study $\bar{M}/S = 0.99$.

Statistical Applications

Three types of standard deviations are computed to see how well the data fit the ellipse. These are:

$$\sigma_{\bar{m}} = \left[\frac{1}{n} \sum_{i=1}^{n} (M_i - \bar{M})^2 \right]^{\frac{1}{2}}$$

$$\sigma_{\bar{m}e} = \left[\frac{1}{n} \sum_{i=1}^{n} (e_i - \bar{M})^2 \right]^{\frac{1}{2}}$$

$$\sigma_e = \left[\frac{1}{n} \sum_{i=1}^{n} (e_i - M_i)^2 \right]^{\frac{1}{2}}$$

where n is the number of measurements (in this case 7). These three types of standard deviation can be used to test for indications of two different properties of the ice in the study area. The first property, homogeniety, will indicate that the ice in the study area behaves as a single unit. The second property, anisotropy, will indicate variation in physical properties of the material with direction.

σe is the best direct measure of scatter in the data. This is true for isotropic as well as anisotropic samples since a sphere is a uniaxial ellipse. If the data fit the ellipse well $\sigma e/S$ is small and precise measurements and homogeniety are both indicated. If $\sigma e/S$ is large then either the measurements are poor, the material inhomogeneous, or both.

Because a circle is a uniaxial ellipse, we always have the relationship $\sigma m > \sigma e$. As the ellipse approaches a circle the eccentricity goes to zero and $\sigma \bar{m} = \sigma e = \sigma \bar{m}e$. Therefore, when all three values are nearly equal, the sample is considered <u>isotropic</u>. However, when $\sigma \bar{m} > \sigma e$ the data fit the ellipse better than a circle and this test indicates anisotropy.

A determination for both anisotropy and homogeniety requires consideration of the two parameters σe and $\sigma\bar{m}e$. If $\sigma e > \sigma\bar{m}e$ the ellipse fits a circle better than it fits the data and this shows either small eccentricity, indicating isotropy, or large data scatter, indicating inhomogeniety, or both. Conversely, if $\sigma\bar{m}e > \sigma e$ the ellipse fits the data better than a circle which means the eccentricity is greater than the scatter of the data.

From the above relationships we have determined that when $\sigma\bar{m} > \sigma e > \sigma\bar{m}e$ the material can be considered non-homogeneously anisotropic. Clearly, $\sigma\bar{m} > \sigma e$ indicates anisotropy and the ratio $\sigma m \geq \sigma e > 1$ is a measure of the amount. The criteria $\sigma e > \sigma\bar{m}e$, coupled with the established anisotropy from $\sigma\bar{m} > \sigma e$, means that the data are scattered either because of inhomogeniety or inaccuracies of measurement, or both. Finally, when $\sigma\bar{m} > \sigma\bar{m}e > \sigma e$ the material can be considered homogeneously anisotropic. In this case the anisotropy is established by $\sigma\bar{m} > \sigma e$ and because $\sigma\bar{m}e > \sigma e$ the data scatter is smaller than the amount of anisotropy it suggests homogeniety.

Only three directional measurements are necessary to define an ellipse, but with only three, no statistical determination can be made to indicate goodness of fit. In our case with seven measurements (more than twice the number necessary), the following values were computed: $M = 2.06 \times 10^7$, $S = 2.08 \times 10^7$, $\bar{m} = 5.13 \times 10^5$, $me = 4.68 \times 10^5$, $e = 2.11 \times 10^5$. The ratio $\sigma e/S$ is about 1%

and indicates precise measurements and homogeniety. The values above show $\sigma m > \sigma\bar{m}e > \sigma e$ and this indicates homogeneous anisotropy in this study area. Here σe is less than 1/2 of the other two types of standard deviation. S is very close to $\bar{M}$ and because the measurements were uniformly distributed over 56^{o} it means the sample quadrant was nearly centered about the point where e and S cross, as is indicated in Figure 22.

The fitted ellipse, e, is plotted with the data in Figure 22 and the fit, as expected from the small value of σe above, is very good. The values at 6^{o} and 16^{o} have large deviations from the theoretical curve. This could be caused by minor local inhomogeniety in this one part of the study area or mean a measurement discrepancy. However, because of the overall good fit of the ellipse curve to the data, the study area is considered homogeneously anisotropic.

To test the individual velocity data (i.e., P, SV and SH-wave velocities) both the P-wave and SV-wave data were plotted against azimuth and a smooth curve estimated through the points. These are shown in Figures 23 and 24. Figure 24 shows both the SV picks and the velocities computed from the Rayleigh wave. The Rayleigh wave velocities were used to estimate the curve because the Rayleigh wave energy arrival was much easier to pick and was considered the more reliable of the two. The curve in Figure 25 was

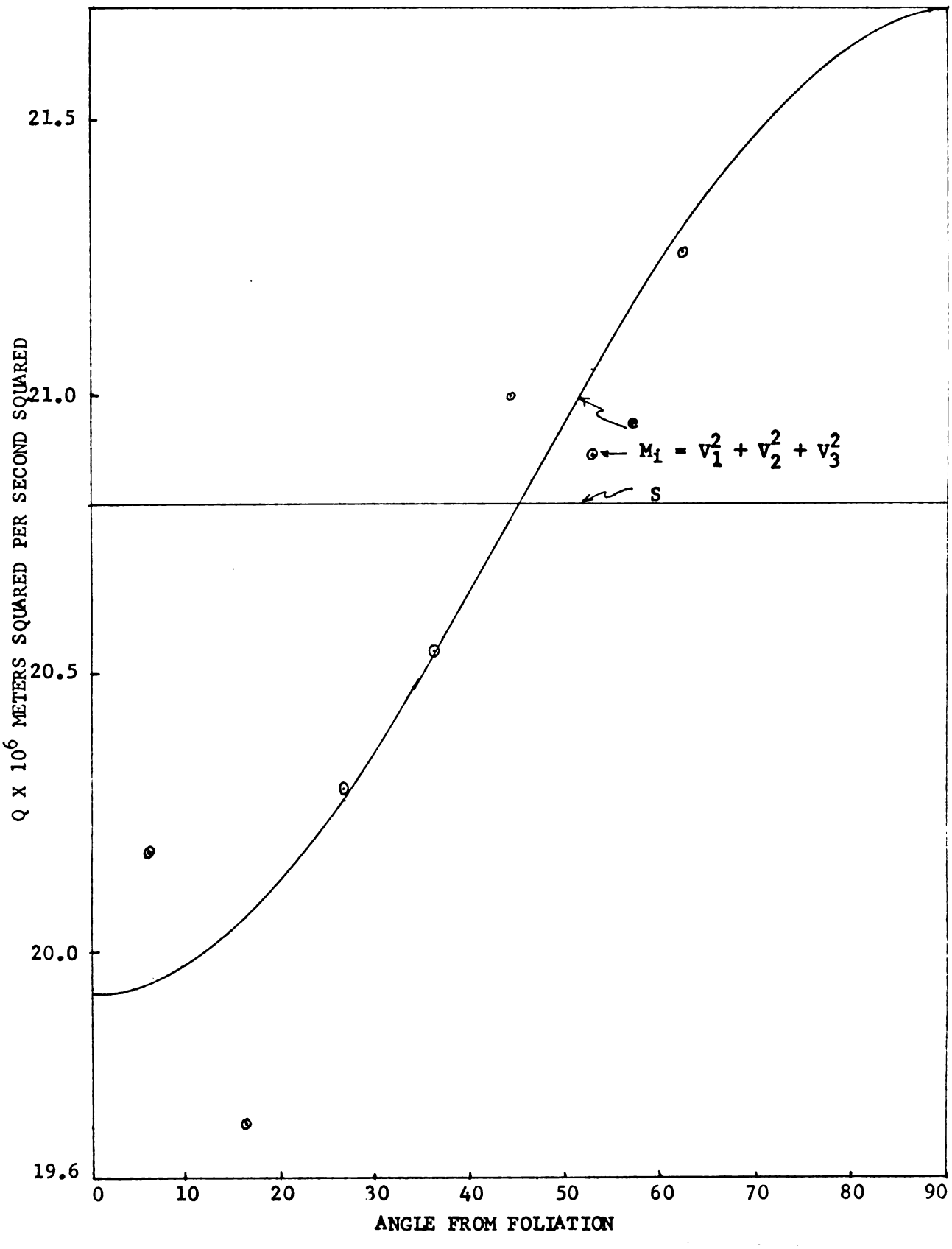

Fig. 21 Q-ellipse theoretical curve with Q data shown by ⊙.

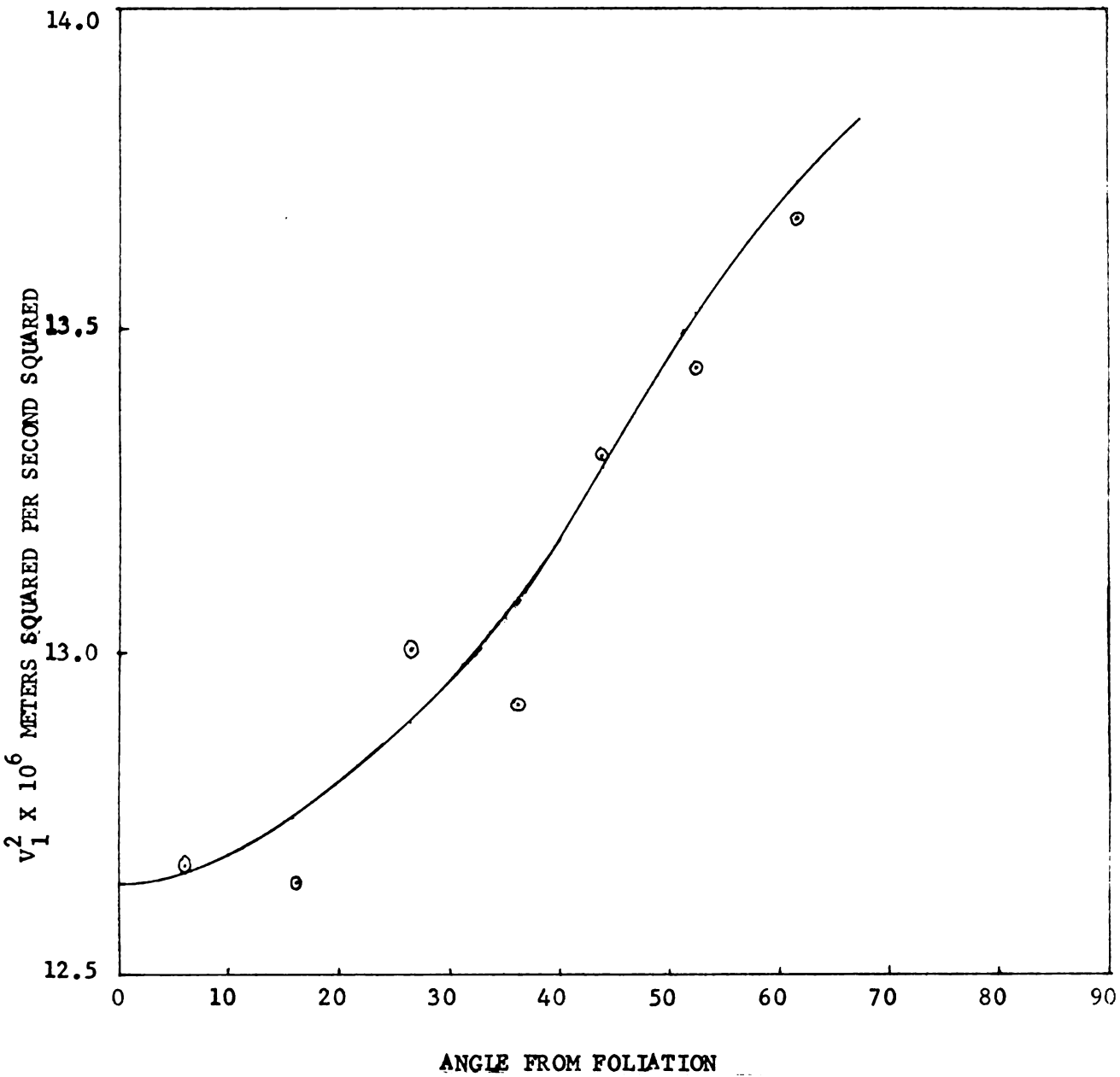

Fig. 22 V_1^2 curve with V_1^2 data points shown by ⊙.

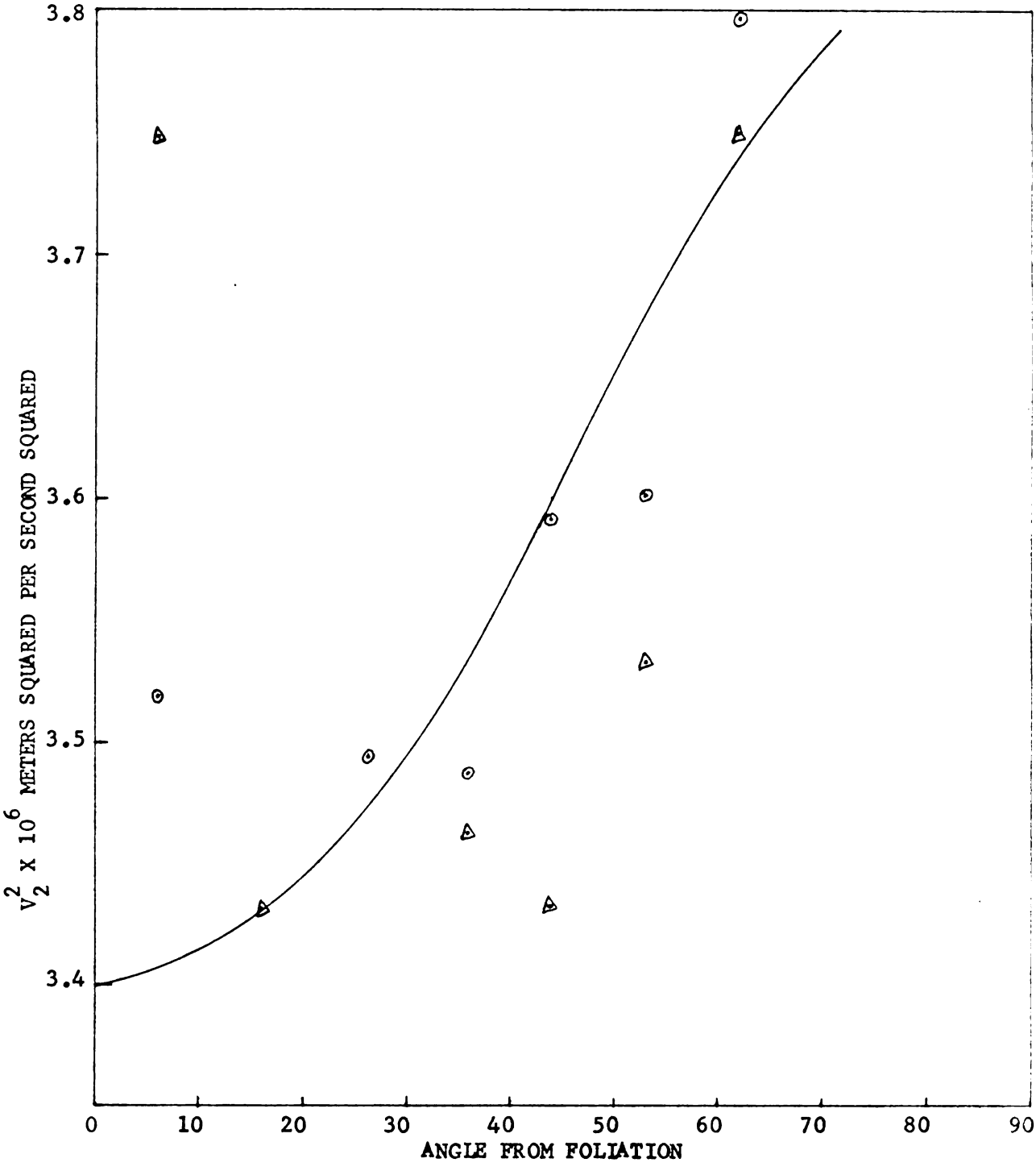

Fig. 23 SV or V_2^2 curve with SV picks shown by Δand Rayleigh velocity divided by .9327 shown by Θ.

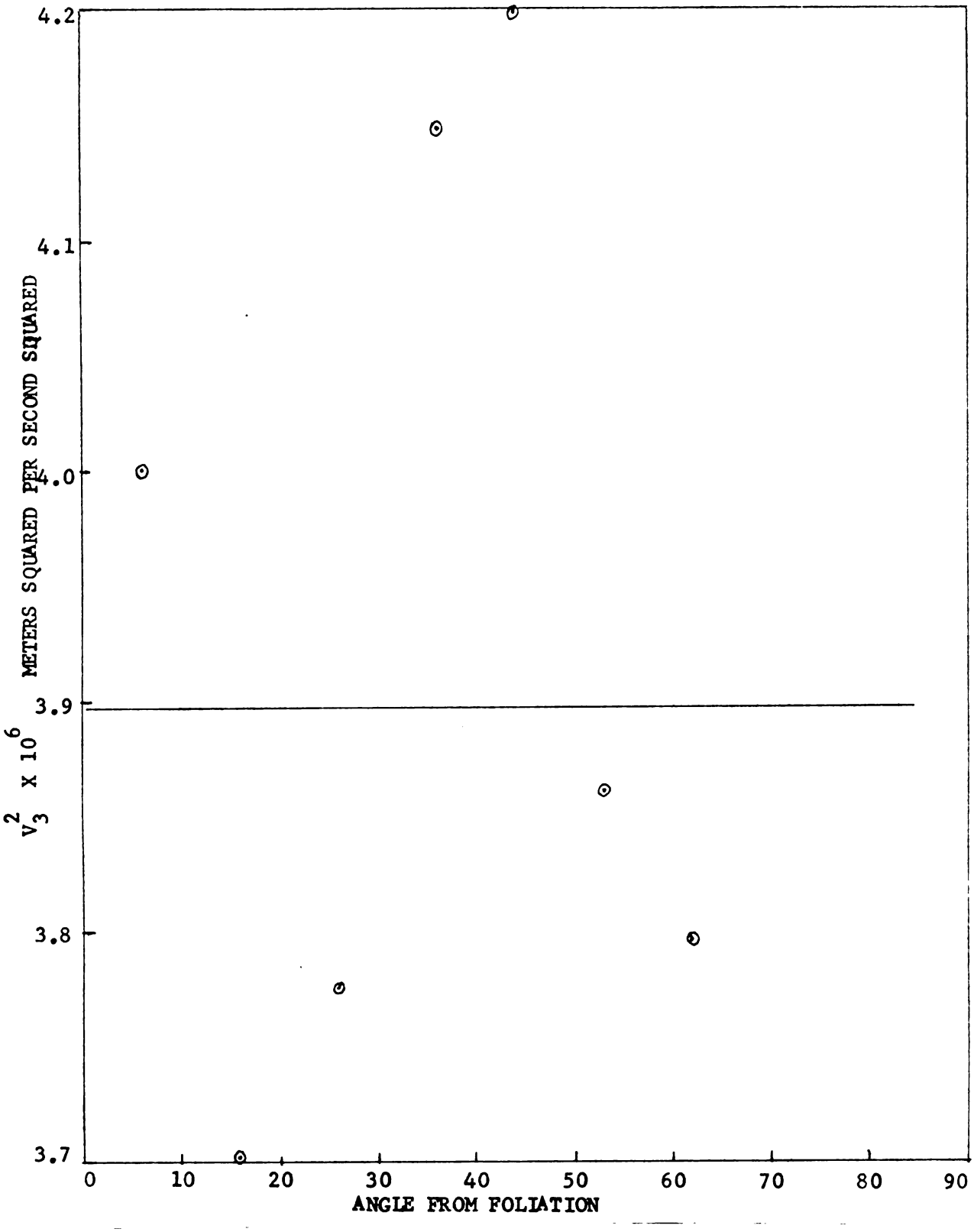

Fig. 24 Q-V_1^2-V_2^2 curve with V_3^2 data shown by θ.

computed from the smoothed values of P and SV and the e data as follows:

$$V_3^2 = e - V_1^2 - V_2^2$$

When the SH velocities were compared to this curve considerable scatter was evidenced. Therefore, the SH-wave velocity data are not of good quality and it is fortunate that these data contribute only about 17% to the Q-ellipsoid calculation.

To determine the orientation of the minor axis of the velocity ellipse the coordinate system was reoriented by hand iteration, changing the direction cosines, until the $\alpha 3$ term in the α matrix approached zero. The angle between the shot 20 heading and the minor axis of the Q-ellipse for this study was about 6.2 degrees. The angle from the foliation to our reference line, the shot 20 heading, was about 10 degrees as measured with the Brunton Compass. The angle between the minor axis and the foliation is therefore 3.8, or more generally, 4 degrees.

The percentage of maximum P-wave velocity anisotropy is calculated from the formula:

$$\% = \frac{2(Vmax - Vmin)}{(Vmax + Vmin)}$$

where Vmax is the maximum and Vmin is the minimum measured P-wave velocity from the raw data in Table 2. The two extremes are about 46° apart and show about 4% P-wave anisotropy.

TABLE 2.--Velocities in meters per second used in the plane ellipse computer program.[1]

Angle	P Wave	S1 Wave	S2 Wave
0.0	3559.22	2000.22	1875.83
9.98	3555.78	1922.83	1832.51
20.17	3610.55	1943.39	1869.12
29.95	3594.15	2036.81	1867.52
37.77	3646.95	2050.06	1895.20
46.45	3666.52	1965.13	1897.41
55.70	3697.27	1948.26	1948.80

[1]P Wave is the compressional-wave velocity; S1 Wave is the Rayleigh wave velocity divided by .9327; and S2 Wave is the SH-wave velocity.

Related Interpretations

Bennett (1968) shows a P-wave curve plotted against angle from the C-axis for an ice crystal. In order for the Vaughan Lewis Glacier P-wave velocity curve to have the same shape as that cited by Bennett, the ice crystal orientation model suggested by petrofabric studies must be reoriented with the C-axes shifted 25° from the normal to the foliation. Rigsby (1960) has reported data from a fold in the Malaspina Glacier that indicates this possibility, because the C-axes maxima are grouped to one side of the point pole. Bennett (1968) also shows curves for 20-, 30- and 40-degree cones with the C-axes evenly distributed

within the cone and with the C-axes also on the surface of the cone. The 20-degree surface cone and 20-, or 30- degree solid cone theoretical curves have the proper form generally to fit the data if the axis of the cone is shifted 25° from the normal to the foliation.

Postma (1956) shows that layering can cause anisotropy. Even though the boundary conditions are not well known the foliation in the ice should qualify as layering (Allen, et al., 1960). This would require a minimum velocity normal to the foliation and definitely does not fit as we see just the opposite in the data (v. Table 2). When the minimum velocity for an ice crystal in the previously cited laboratory tests is compared with the minimum velocity from the field data, the Vaughan Lewis Glacier velocity is slower (i.e., a minimum P-wave velocity for the test crystal of 3803 meters per second vs. a minimum of 3555 meters per second for this field study). The layering effect can explain some of the discrepancy but low density and poor acoustical coupling from ice crystal to ice crystal would also be needed to explain this considerable velocity difference.

Maximum P-wave velocity anisotropy over a 46° area in the study zone is 4%. Bennett (1968) shows a maximum velocity difference through 52° of 7%. Assuming a C-axes orientation that is 25° from the normal to the foliation, the study area anisotropy is only two-thirds its expected value. As the layering affects anisotropy in the opposite

sense of the C-axes preferred orientation, a combination of strong crystal orientation with weak layering effect may give the proper amount of anisotropy. This means, however, a complex crystal orientation (because of a 25° reorientation) and layering (because of the low P-wave velocity) are both affecting the P-wave velocity of the glacier ice in the study area.

CONCLUSIONS

Because the relationship $\sigma\bar{m} > \sigma me > \sigma e$ is satisfied by the field data, the glacier ice in the study area is considered to be homogeneously anisotropic. The material is thus behaving as a single homogeneous unit and does not display the variations which would be expected in a random material. In turn this suggests that the physical change with direction is in fact related to fabric, to micro-structure or to macro-structure, or to combinations of all three.

The minor axis of the Q-ellipse was determined to be within 4^{o} of the foliation, showing that the effect of crystal orientation is the dominant factor in this section of the glacier. This conclusion is based on the fact that the layering model predicts the lowest P-wave velocity normal to the foliation.

The P-wave velocity curve of the field data over the 56 degrees measured has the proper form to fit the P-wave velocity curve shown by Bennett (1968) for a single crystal. To align the two curves the oriented C-axis model must be shifted 25^{o} from the normal to the foliation.

The shear data are actually not good enough to match with theoretical curves, calculated for C-axes orientation, to check this conclusion. It is believed, therefore, that because of the necessity of a 25° shift, the crystal orientation must be rather complex.

The percentage of anisotropy from the P-wave data over 46° amounts to 4% which is about two-thirds the expected amount, assuming a model with crystal C-axes alignment 25° from the normal to the foliation. Either a combination of the layering effect and the C-axes orientation effect, or only a complex C-axes orientation effect, can explain this low % anisotropy. The C-axes orientation randomly distributed within a 20-degree cone, or on the surface of a 20- or 30-degree cone, probably would have the necessary percentage of P-wave anisotropy. Therefore all that can be concluded in this regard is that either the effect of a complex orientation of the crystals or a layering effect or both is reducing the percentage of velocity change.

The minimum P-wave velocity of the field data is 245 meters per second slower than the minimum velocity found in laboratory tests on an ice crystal. This can be accounted for by both poor acoustical coupling between crystals and a layering effect coupled with the C-axes orientation. The layering anisotropy is opposite the C-axes orientation anisotropy and would therefore lower

the P-wave velocity as well as decrease the amount of P-wave anisotropy.

Complex crystal orientation is the dominate factor in the anisotropy, but a layering effect is also present and is helping lower the P-wave velocity.

The last conclusion is that better techniques for the generation of seismic shear-wave energy in the field need to be developed. Hopefully a better shear-wave generator can be developed to produce polarized energy sufficient to measure velocities in ice over long distances. With better shear-wave measurements coupled with uniformly distributed measurements over 180^{o} the crystal effect could then be separated from the structural effect by matching theoretical curves based on model and laboratory tests on ice crystals with the curves measured in the field. Also, a glacier with a single known stress field should be measured in further development of this technique.

REFERENCES

Allen, C. R.; Kamb, W. B.; Meier, M. F.; and Sharp, R. P. (1960). Structure of the Lower Blue Glacier, Washington. Jour. Geology, v. 68, no. 6, p. 601-625.

Bennett, H. F. (1968). An investigation into velocity anisotropy through measurements of ultrasonic wave velocities in snow and ice cores from Greenland and Antarctica. University of Wisconsin (unpublished Ph. D. thesis).

Bennett, H. F. (1972). A simple seismic model for determining principle anisotropic direction. A. G. U. June 10, 1972. (In press.)

Chrzanowski, A. (1968). Glacier mapping on the Juneau Icefield, Alaska-British Columbia. (abs.) Proceedings of the Alaska Science Conference, 19th, Whitehorse, Y. T., Canada.

Dittrich, W. A. (1972). Surface velocity analyses on the Vaughan Lewis Glacier, Alaska, 1970, 1971. Proceedings of the Arctic and Mountain Environments Symposium, Michigan State University; 22-23 April 1972. (In press.)

Freers, T. F. (1965). Preliminary structural glaciological investigation of the wave-bands on the Vaughan Lewis Glacier, Alaska. (abs.) Michigan Acad. Sci., Arts and Letters, Ann Arbor.

Freers, T. F. (1968). A structural and morphogenetic investigation of the Vaughan Lewis Glacier and adjacent sectors of the Juneau Icefield, Alaska 1961-1964. Michigan State Univ. (unpublished M.S. thesis).

Gow, A. J. (1963). Results of measurements in the 309 Meter Bore Hole at Byrd Station, Antarctica. Jour. of Glaciology, v. 4, Nov. 36, Oct. 1963.

Gow, A. J. (1964). The inner structure of the Ross Ice Shelf at Little America, Antarctica, as revealed by deep core drilling. IASH Commission on Snow and Ice, Pub. No. 61, p. 272.

Green, R. E. and MacKennon, L. (1956). Determination of the elastic constance of ice single crystals by an ultrasonic pulse method. Jour. of the Acoustical Society of America, v. 28, no. 6, p. 1292.

Havas, T. W. (1965). Surface velocity and strain-rate measurements on several Alaskan glaciers, 1964. Michigan State Univ. (unpublished M.S. thesis).

Jaeger, J. C. (1956). Elasticity, Fracture and Flow. John Wiley and Sons.

Kamb, W. B. (1959). Theory of preferred crystal orientation developed by crystallization under stress. Jour. Geology, v. 67, p. 153-170.

Kamb, W. B. (1961). The glide direction in ice. Jour. Glaciology, v. 3, no. 30, p. 1097.

Kittredge, T. F.; Freers, T. F.; and Havas, T. (1965). Structure and deformation study of wave-ogives on the Vaughan Lewis Glacier, Juneau Icefield, Alaska. Proceedings of the Alaska Sci. Cong., 16th, Juneau, Alaska.

Kittredge, T. R. (1967). Formation of wave-ogives below the Icefall of the Vaughan Lewis Glacier, Alaska. Univ. of Colorado (unpublished M.S. thesis).

Knopoff, L. (1952). On Rayleigh wave velocities. Seis. Soc. of America Bull., v. 42, p. 307-308.

Miller, Keinz. (1972). An electrical resistivity investigation of subsurface structures on the Lemon and Ptarmigan Glaciers, Juneau Icefield, Alaska. Proceedings of the 1972 Arctic and Mountain Environments Symposium, Michigan State University, 22-23 April 1972. (In press.)

Miller, L. R.; Pinchak, A.; Trabant, D.; and Trent, D. (1968). Some 1967 and 1968 measurements on surface bulges and englacial structures of the Vaughan Lewis Glacier, Alaska. (abs.) Alaska Sci. Conf., 19th, Whitehorse, Y. T., Canada.

Miller, L. R. (1970). Englacial structures of the Vaughan Lewis Glacier, Juneau Icefield, Alaska, 1967-1969. Michigan State Univ. (unpublished M.S. thesis).

Miller, M. M. (1952). Scientific observations of the Juneau Icefield Research Project, Alaska, 1949 field season. American Geographical Society, J.I.R.P. Report No. 6, 200 pp., 43 figures.

Miller, M. M. (1955). A nomenclature for certain englacial structures. Acta Geographica, v. 14, no. 17, p. 291-299.

Miller, M. M. (1956). The glaciology of the Juneau Icefield, Southeastern Alaska, with special references to the Taku Anomaly. O.N.R. Contract (83,001).

Miller, M. M. (1963). Taku Glacier evaluation study. State of Alaska Department of Highways, Jan. 1963.

Miller, M. M. (1968). Theory of Wave-Ogive formation on the Vaughan Lewis Glacier, Northern Boundary Range Alaska-British Columbia. (abs.) Symposium on Surging Glaciers and their Geologic Effects, Nat. Research Council of Canada, Banff, Alberta, June, 1968.

Miller, M. M.; Freers, T. F.; Kittredge, T. F.; and Havas, T. (1968). Wave-Ogive formation and Associated Phenomena on the Vaughan Lewis and Gilkey Glaciers, Juneau Icefield, Alaska. (abs.) Alaska Sci. Conf., 19th, Whitehorse, Y. T., Canada.

Nye, J. F. (1957). Physical Properties of Crystals. Oxford: Clarendon Press.

Paterson, W. S. B. (1969). The Physics of Glaciers. Pergamon Press.

Postma, G. W. (1955). Wave propagation in a stratified medium. Geophysics, v. 20, no. 4, p. 780-806.

Poulter, T. C.; Allen, C. F.; and Miller, S. W. (1949). Seismic measurements on the Taku Glacier. Stanford Research Institute, Stanford, California.

Poulter, T. C.; Prather, B. W.; Shaw, R. M.; and Walasek, S. (1967). Geophysical depth profiles on the Juneau Icefield, Alaska, 1965-67. (abs.) Alaska Sci. Conf., 17th, Fairbanks, Alaska, 1967.

Prather, B. W.; Schoen, L.; Classen, D.; and Miller, H. (1968). 1968 seismic depth measurements on the Taku, Vaughan Lewis and Lemon Glaciers, Alaska. (abs.) Alaska Sci. Conf., 19th, Whitehorse, Y. T., Canada.

Prather, B. W. and Bennett, H. F. (1972). Anisotropic effects on seismic velocities of certain Alaskan Glaciers. Proceedings of the 1972 Arctic and Mountain Environments Symposium, Michigan State University, 22-23 April, 1972. (In press.)

Rigsby, G. P. (1951). Crystal fabric studies on Emmons Glacier, Mount Rainier, Washington. Jour. Geology, v. 59, no. 6, p. 590-598.

Rigsby, G. P. (1960). Crystal orientation in glacier and in experimentally deformed ice. Jour. Glaciology, v. 3, no. 27, p. 589.

Shaw, R. M.; Hinze, W. J.; and Asher, R. A. (1972). Gravity surveys on the Lemon and Ptarmigan Glaciers, 1971. Proceedings of the 1972 Arctic and Mountain Environments Symposium, Michigan State University, 22-23 April, 1972. (In press.)

Shumski, P. A. (1964). Principles of Structural Glaciology, Dover Publications.

Steinemann, S. (1954). Flow and recrystallisation of ice. ISAH Commission on Snow and Ice, Pub. No. 39, p. 449., 1958.

Tallman, A. T. (1972). Frost mound and palsa investigations using electrical resistivity. Proceedings of the 1972 Arctic and Mountain Environments Symposium, Michigan State University, 22-23 April, 1972. (In press.)

Thiel, E.; LaChappelle, E. R.; and Behrendt, J. C. (1957). The thickness of Lemon Creek Glacier, Alaska, as determined by gravity measurements. A.G.U., v. 38, no. 5, p. 745-749.

Whitaker, James T. (1966). Ultrasonic velocity measurements of precambrian metamorphic rocks and their correlations with field measurements. Michigan State Univ. (unpublished M.S. thesis).

APPENDIX

PLANE ELLIPSE TWO-DIMENSIONAL COMPUTER PROGRAM WITH INSTRUCTIONS AND DECK DIAGRAM

This program is written in fortran and the data are inserted between the last 789 and 6789 cards. Provisions in the data deck include an AN or angle term in the first data card. The angle should be a floating point number of not more than 9 digits and should be entered along with a decimal point in the first 10 spaces of the card. Any positive angle up to 360^{o} can be used. The AN term can be used to hand iterate the axes of the ellipse so that the term approaches a small value. Then the AN term is the $\alpha 3$ angle between the fixed reference point and the minor axis of the ellipse. If no orientation is desired a zero must be entered.

The next card tells how many measurements, n, are to be used. For the two dimensional case that this specific program is written for n cannot be less than three.

After the n card comes a data card for each direction measured. P, SV and SH have 20 spaces each, followed by the angle from some fixed reference point, in this study

the shot 20 heading, in the last 20 spaces to fill the card. These are all floating point numbers and anywhere in the 20 spaces the number with a decimal point can be entered.

The only card that needs to be changed other than in the data deck is the DIMENSION statement, provided n is something other than seven. In that case the sevens should be replaced by n making certain that the threes are not changed. This statement tells the computer how much memory to reserve for the variables referenced and it is important that only enough room be provided.

The two cards in the DIMENSION statement are enlarged so the reader can see which variables in the computer program have memory reserved. The statement on the first card which starts in column 7 and ends in column 72 is as follows:

```
DIMENSION A(7), THETA(7,3), THETA1(3,3),
CATINV(3,3), THETA2(3,7), ALPH
```

A G (any symbol could have been used) is placed in column 6 of the second card so the statement from the first card will continue as follows:

```
GA(3), V(7,3), D(7,2), THETAT(3,7), EQ(7), AZ(7)
```

where the sevens represent the number of measurements n.

DECK STRUCTURE

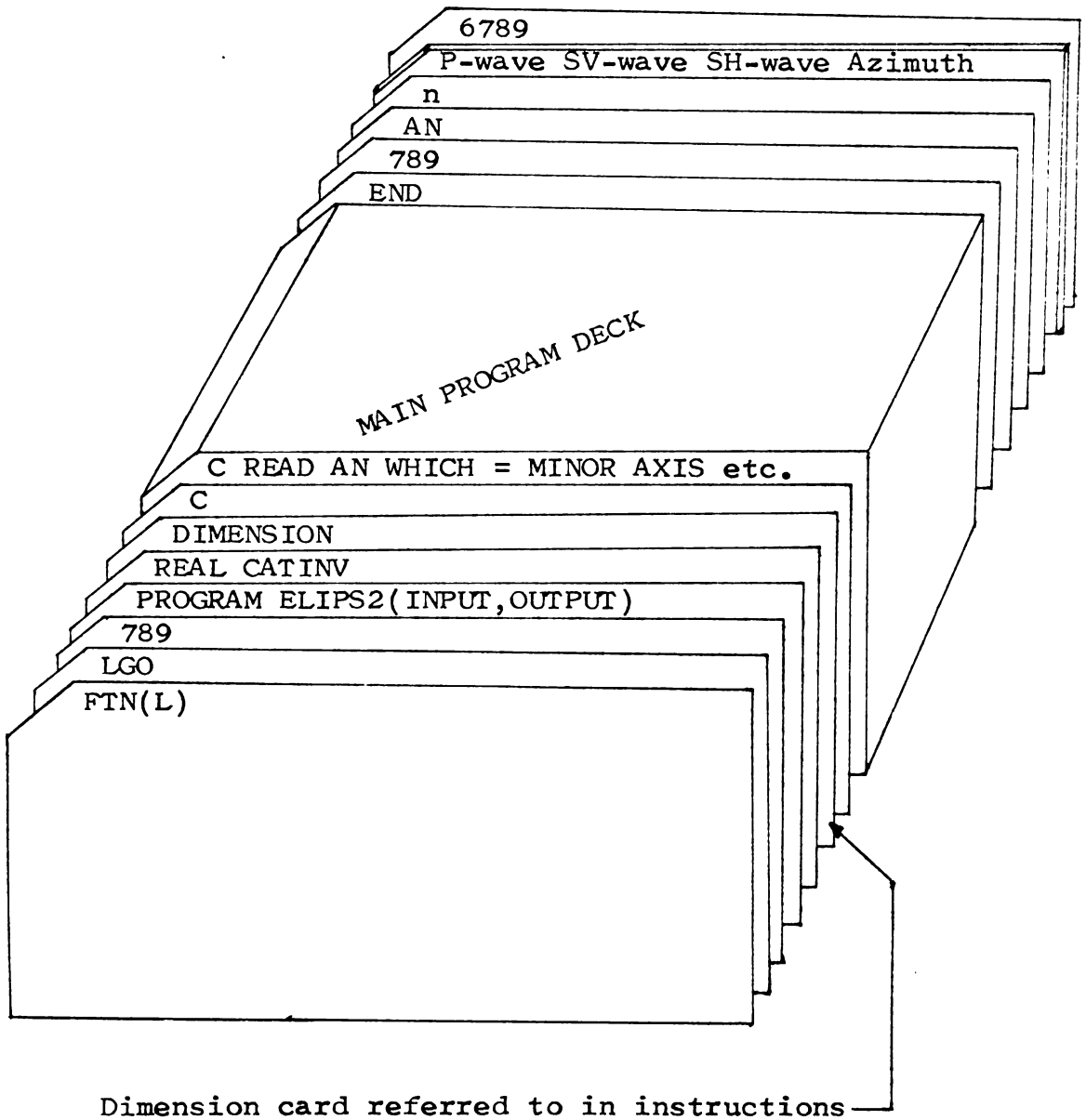

```
      PROGRAM ELIPS2(INPUT,OUTPUT)
      REAL CATINV
      DIMENSION A(7),THETA(7,3),THETA1(3,3),CATINV(3,3),THETA2(3,7),ALPH
     GA(3),V(7,3),D(7,2),THETAT(3,7),EQ(7),AZ(7)
C
C READ AN WHICH = MINOR AXIS ORIENTATION FROM SELECTED FIXED REFERENCE
C
      READ169,AN
169   FORMAT(F10.5)
C
C  READ N WHICH = NUMBER OF MEASUREMENTS
C
      READ100,N
100   FORMAT(I6)
      EIP=3.141592653
C
C READ P, SV AND SH VELOCITIES AND CORRESPONDING AZIMUTH,20 SPACES EACH
C
      DO11I=1,N
      READ102,V(I,1),V(I,2),V(I,3),AZ(I)
102   FORMAT(4F20.10)
11    CONTINUE
      DO99I=1,N
      D(I,1)=COS(EIP*(AZ(I)+AN)/180)
      D(I,2)=SIN(EIP*(AZ(I)+AN)/180)
99    CONTINUE
      PRINT200
200   FORMAT(1H1,10X,27HDIRECTION COSINES, MATRIX D,9X,7HAZIMUTH,//,10X,
     11HX,14X,1HY,/)
      DO20I=1,N
      PRINT201,(D(I,1),D(I,2),AZ(I))
201   FORMAT(1H0,5X,F10.9,4X,F10.9,20X,F10.3)
20    CONTINUE
      PRINT96,(AN)
96    FORMAT(1H0,17HORIENTATION ANGLE,F10.5)
      PRINT205
```

```
205   FORMAT(1H0,10X,41HVELOCITIES IN METERS PER SECOND, MATRIX V//10X,6
     GHP WAVE12X7HS1 WAVE10X7HS2 WAVE//)
      DO21I=1,N
      PRINT202,(V(I,J),J=1,3)
202   FORMAT(1H0,5X,(3F15.5,10X))
21    CONTINUE
C
C     GENERATING THE THETA MATRIX
C
      DO1I=1,N
      THETA(I,1)=D(I,1)**2
      THETA(I,2)=D(I,2)**2
      THETA(I,3)=(2*D(I,1))*D(I,2)
1     CONTINUE
      PRINT206
206   FORMAT(1H1,10X,12HTHETA MATRIX//)
      DO22I=1,N
      PRINT210,(THETA(I,J),J=1,3)
210   FORMAT(1H0,5X,(3F15.5,10X))
22    CONTINUE
C
C     GENERATING *A* MATRIX
C
      DO2I=1,N
      A(I)=(((V(I,1)**2)+(V(I,2)**2))+(V(I,3)**2))
2     CONTINUE
      PRINT204,A
204   FORMAT(1H110X8HA MATRIX,//,(10X,F20.10//))
C
C GENERATING THETA1 MATRIX, WHICH IS THETA MATRIX TIMES ITS TRANSPOSE
C
      DO50I=1,3
      DO50J=1,N
      THETAT(I,J)=THETA(J,I)
50    CONTINUE
      PRINT230
```

```
230   FORMAT(1H1,10X,15HTHETA TRANSPOSE//)
      DO40I=1,3
      PRINT231,(THETAT(I,J),J=1,N)
231   FORMAT(1H0,5X,(9F10.5,7X))
40    CONTINUE
      DO3I=1,3
      DO3J=1,3
      SUM=0
      DO7K=1,N
      THETA1(I,J)=THETAT(I,K)*THETA(K,J)
      SUM=SUM+THETA1(I,J)
7     CONTINUE
      THETA1(I,J)=SUM
3     CONTINUE
      PRINT220
220   FORMAT(1H1,10X,13HTHETA1 MATRIX//)
      DO30I=1,3
      PRINT221,(THETA1(I,J),J=1,3)
221   FORMAT(1H0,5X,(3E12.5,8X))
30    CONTINUE
C
C     SUBRQUTINE TO GENERATE INVERSE
C
      M=3
      CALL BNVMAT(M,THETA1,CATINV,DETM)
      PRINT300,(DETM)
300   FORMAT(1H5,10X,13HDETERMINATE B,4X,F10.5)
C
C     GENERATING THETA2 MATRIX, WHERE THETA2 MATRIX IS INVERSE TIMES
C     THETA TRANSPOSE
C
      DO4I=1,3
      DO4J=I,N
      SUM=0
      DO6K=1,3
      THETA2(I,J)=CATINV(I,K)*THETAT(K,J)
      SUM=SUM+THETA2(I,J)
6     CONTINUE
```

```
      THETA2(I,J)=SUM
4     CONTINUE
C
C     GENERATING ALPHA MATRIX
C
      DO5I=1,3
      SUM=0
      DO8K=1,N
      ALPHA(I)=THETA2(I,K)*A(K)
      SUM=SUM+ALPHA(I)
8     CONTINUE
      ALPHA(I)=SUM
5     CONTINUE
      PRINT222
222   FORMAT(1H1,10X,17HINVERSE OF THETA1//)
      DO31I=1,3
      PRINT223,(CATINV(I,J),J=1,3)
223   FORMAT(1H0,5X,(3E15.5,10X))
31    CONTINUE
      PRINT224
224   FORMAT(1H1,10X,13HTHETA2 MATRIX//)
      DO32I=1,3
      PRINT225,(THETA2(I,J),J=1,N)
225   FORMAT(1H0,5X,(9E12.5,8X))
32    CONTINUE
      PRINT203,ALPHA
203   FORMAT(1H110X12HALPHA MATRIX//(10X,E20.10/))
C
C COMPUTE Q FOR CIRCLE 1,2, AND ELLIPSE
C
      CIRCS=(ALPHA(1)+ALPHA(2))/2
      DO301 I=1,N
      EQ(I)=(D(I,1)**2)*ALPHA(1)+D(I,2)*D(I,1)*ALPHA(3)*2+(D(I,2)**2)*AL
     1PHA(2)
      PRINT302,(I,EQ(I))
302   FORMAT(1H0,5X,8HI EQUALS,2X,I4,10X,16HELLIPSE Q EQUALS,2X,F20.10)
```

```
301   CONTINUE
      SUM=0
      DO303I=1,N
      SUM=SUM+A(I)
303   CONTINUE
      CIRCM=SUM/N
      PRINT310,(CIRCS,CIRCM)
310   FORMAT(1H0,//,12HQ FROM ELIPS,F20.10,10HQ FROM *A*,F20.10)
C
C COMPUTE 5 MEAN SQUARE DEVIATIONS
C
      SUEM=0
      SUMM=0
      SUMS=0
      SUMES=0
      SUME=0
      DO304I=1,N
      DELTS=(A(I)-CIRCS)**2
      DELTES=(EQ(I)-CIRCS)**2
      DELTME=(EQ(I)-A(I))**2
      DELTMM=(A(I)-CIRCM)**2
      DELTEM=(EQ(I)-CIRCM)**2
      SUMM=SUMM+DELTMM
      SUEM=SUEM+DELTEM
      SUMS=SUMS+DELTS
      SUMES=SUMES+DELTES
      SUME=SUME+DELTME
304   CONTINUE
      DEVEM=SQRT(SUEM/N)
      DEVMM=SQRT(SUMM/N)
      DEVS=SQRT(SUMS/N)
      DEVES=SQRT(SUMES/N)
      DEVME=SQRT(SUME/N)
      PRINT305
      PRINT306,(DEVMM,DEVS,DEVME,DEVES,DEVEM)
```

```
305   FORMAT(1H1,8HSIGMA  M,6X,8HSIGMA  S,6X,8HSIGMA  E,6X,8HSIGMA SE,6X
     G,8HSIGMA ME,//)
306   FORMAT(1H0,5E14.5)
      STOP
      END
      SUBROUTINE BNVMAT(N,B,BI,DET)
      DIMENSION B(3,3), BI(3,3)
C
C FINDS INVERSE AND DETERMINANT OF MATRIX B OF ORDER N BY PIVOTAL CONDENSATION
C N=DIM. MATRIX B. BI=INVERSE OF B. DET=DETERMINANT OF B
C
      A=1.0
C
C     GENERATE INDENTITY MATRIX
C
      DO 15 I=1,N
      DO15 J=1,N
15    BI(I,J)=0.0
      DO 20 I=1,N
20    BI(I,I) = 1.0
C
C     BEGIN PIVOTAL CONDENSATION
C     J IS THE  PIVOTING ROW
C
      DO 60 J=1,N
      P=B(J,J)
      A=A*P
C
C     DIVIDE PIVITING ROW BY DIAGONAL ELEMENT
C
      DO 47 K=1,N
      B(J,K)=B(J,K)/P
47    BI(J,K)=BI(J,K)/P
C
C     I IS THE ROW TO BE REDUCED
C
```

```
      DO 55 I=1,N
      IF(I.EQ.J) 55,50
50    SAVE=B(I,J)
      DO 53 M=1,N
      B(I,M)=B(I,M)-B(J,M)*SAVE
53    BI(I,M)=BI(I,M)-BI(J,M)*SAVE
55    CONTINUE
60    CONTINUE
      DET=A
      RETURN
      END
```

VELOCITIES IN METERS PER SECOND, MATRIX V

P WAVE	S1 WAVE	S2 WAVE
3559.22000	2000.22000	1875.83000
3555.78000	1922.83000	1832.51000
3610.55000	1943.39000	1869.12000
3594.15000	2036.81000	1867.52000
3646.95000	2050.06000	1895.20000
3666.52000	1965.13000	1897.41000
3697.27000	1948.26000	1948.80000